University of Zurich[UZH]

Impact of mechanical loosening on physical soil properties in a severely compacted subsoil

GEO 511 Master's Thesis

Author
Alina Widmer
15-701-345

Supervised by
Johannes Koestel (johannes.koestel@agroscope.admin.ch)

Faculty representative
PD Dr. Guido Lars Bruno Wiesenberg

25.08.2022
Department of Geography, University of Zurich

Abstract

Compacted soils occur widely in agricultural lands and bring a multitude of challenges. A possible alleviation method is the mechanical loosening of these soils. However, according to the literature, mechanical loosening has not always yielded improvements in soil structure. This thesis investigated the effect of mechanical loosening on the soil structure and the physical properties of a severely compacted subsoil. During construction work, a field in Changins was used as a deposit for excavated material over several years, which led to a high level of subsoil compaction. After the deposit was removed, the soil was loosened mechanically. Penetration resistance was assessed with a penetrologger before loosening and with a penetrometer one and a half years after loosening. One year after the loosening, soil samples were collected from the still compacted, the loosened, and the reference plots and scanned with X-rays. From the resulting 3D images (resolution $>$126 μm), changes in soil matrix density and morphological measures of the imaged pore network were studied. In the laboratory, air diffusion and air permeability were measured at -30 hPa, -100 hPa, and -300 hPa matric potential. The results suggested that the reference plots, assumed to have experienced no compaction, were moderately compacted. Mechanical loosening decreased penetration resistance, partially decreased soil matrix density, and increased macroporosity at 60 cm depth. However, the connectivity of macropores was not restored. Percolation of the macropore network did not improve after loosening, and neither did air permeability at -30 and -100 hPa. Only at smaller pore diameters (9-28 μm) increased air permeability and air diffusion were found in the loosened plots. A year after loosening, biopores were not restored, which might explain the low connectivity. Hence, local anoxic conditions under high moisture levels (field capacity) may appear in the soil, which does not favor root growth and aerobic microbial life. The improvements in mechanical loosening were strongest, where the highest level of compaction was previously found (60 cm depth). Although some parameters showed significant alleviation, mechanical loosening could not fully restore a firmly compacted soil within one year. Soil structure recovery progresses slowly since natural restoring mechanisms are slow. Mechanical loosening only supports and cannot replace them. Since the success of mechanical loosening cannot always be guaranteed and soil structure recovery remains a slow process, the focus should lie on prevention of compaction.

Acknowledgements

I would like to thank John Koestel, who supported me and somehow always found the time when I needed help. Additionally, I thank Guido Wiesenberg for his helpful tips and support. I am grateful to Marlies Sommer for measuring the air permeability and air diffusion and for patiently explaining the measurement devices to me. Furthermore, I am very thankful for the help of Maria Vorkauf and Valerio Volpe in X-ray imaging. Special thanks go to Thomas Renggli, who was a great help with Python. I am grateful to Alice Johannes, who organized the writing retreats in which I wrote most of my thesis. Additionally, I would like to thank the people of the BQBN group and my soil mates in the C250 office. Last but not least, I wish to express my gratitude to my friends, family, and boyfriend, who supported me in every way possible.

Contents

List of Figures

Photographs of the title page were provided by Alice Johannes.

List of Tables

List of Abbreviations

ROCSUB	**R**estoration **O**f a **C**ompacted **SUB**soil
POM	**P**articulate **O**rganic **M**atter
CT	**C**omputed **T**omography

Chapter 1

Introduction

1.1 Consequences of soil compaction

Soil compaction is one of the main challenges of modern agriculture. In the Netherlands, 43 % of the agricultural land is affected by compaction (Brus and Akker, 2018). Evidence suggests that the impacted area accounts for 25 % of the arable land in Europe (Schjønning et al., 2015). Grazing of animals in large numbers, mining, and construction work are possible causes of soil compaction (Batey, 2009; Spoor, 2006). Naturally compacted soils like iron pans in podsols exist as well (Batey and McKenzie, 2006). However, the main reason for the broad occurrence of compacted soils is the intensification of agriculture, which led to an increase in farm vehicle weight (Keller et al., 2019). Today's farm machinery weight is approaching the weight of sauropods which once walked the Earth (Keller and Or, 2022). This puts arable soils under alarmingly high pressure and makes soil compaction a very current issue (Keller and Or, 2022).

Soil compaction strongly affects soil structure which is the property, that describes the state of a pore system and its channels in the soil (Weil and Brady, 2017). A healthy soil structure is characterized by well-connected pores and stable aggregates that enable water and nutrient flow and aeration for roots and microbes (Zhang et al., 2021). During soil compaction, particles are pressed together and aggregates are crushed or combined into larger aggregates (Batey, 2009; DeJong-Hughes, 2018). This leads to an increase in soil bulk density, larger soil cohesion, fewer large pores (macropores), and reduced pore connectivity (Hamza and Anderson, 2005; Hemmat and Adamchuk, 2008; Tarawally et al., 2004). Since macropores efficiently transport water and air in the soil system, air and water infiltration and nutrient transport are limited in a compacted soil (Hemmat and Adamchuk, 2008; Keller et al., 2021; Schäffer et al., 2007). Although signs of compaction occur in a broad range of soils and climates, soils with low organic matter content, fine texture, and intensive agriculture are especially vulnerable (Hamza and Anderson, 2005).

Soils provide vital ecosystem services to the human civilization and terrestrial life (Figure 1.1). Under compaction, four of these services are strongly reduced: water

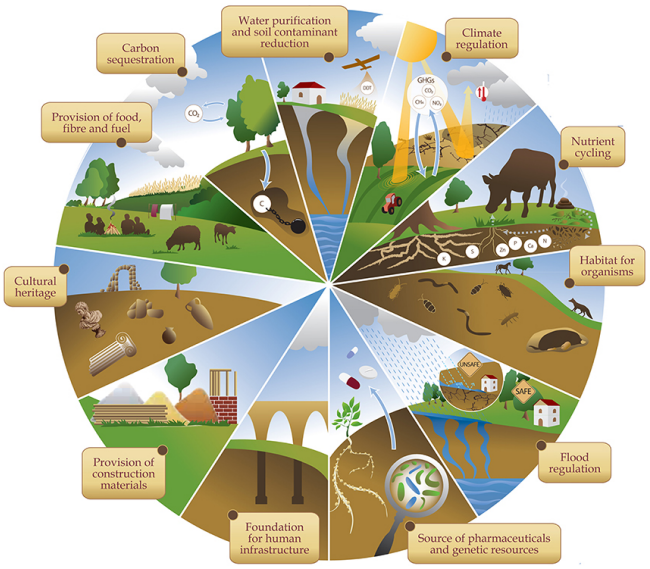

FIGURE 1.1: Ecosystem services provided by soils (FAO and ITPS, 2015).

purification and storage, provision of food, nutrient cycling, and habitats for organisms. Due to limited gas diffusion, the soil is not habitable for aerobic organisms anymore (Berisso et al., 2012; Drew, 1992). Furthermore, root growth is restricted at penetration resistances above 2.5 MPa (Gao et al., 2016a). Reduced root growth leads to lowered nutrient cycling efficiency (Hammel, 1994; Kautz et al., 2013). With limited rooting depth and reduced water availability, crop growth is similarly restricted, which leads to a reduction of yield (Chen and Weil, 2010; Keller et al., 2019; Wahlström et al., 2021). A compacted soil has a reduced water storage capacity due to a lowered porosity (Keller et al., 2019). With drought intensity and frequency expected to increase in the light of climate change, compacted soils offer a reduced water stress resilience (Batey, 2009; IPCC, 2022). Additionally, soil compaction enhances preferential water flow, which lowers the water purification ability of soils and might lead to increased pesticide and fertilizer outwash to nearby water bodies and groundwater (Jarvis, 2007). Since soil compaction affects physical, biological, and chemical soil properties, the sum of all these effects can lead to significant soil degradation (Batey, 2009).

According to the environmental legislation of Switzerland (UGS, SR 814.01 of 07.10.1983), physical soil stress is only allowed to a level where soil fertility is still ensured. A soil is regarded as fertile if it inheres sufficient biological activity, an intact soil structure, and shows the ability for decomposition of organic material (VBBo), SR 814.12 of 01.07.1998). However, soil protection in Switzerland focuses mainly on chemical aspects and few guidelines on protection of soil structure have been published so far, let alone threshold values (Johannes et al., 2021b).

1.2 Subsoil structure recovery

The subsoil is located below the topsoil (A-horizon) and is often called B-horizon (Figure 1.2). Subsoils are characterized by a lower biological activity, lower soil organic matter content and lower temperature variations (Håkansson and Reeder, 1994; Weil and Brady, 2017). Mostly, subsoils have a large volume, where water and nutrients are stored, readily available for plant roots (Kautz et al., 2013).

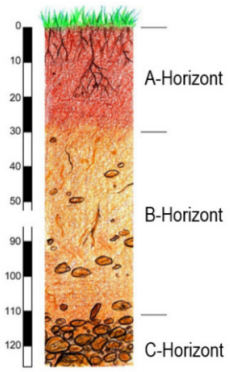

FIGURE 1.2: Example of a common soil profile (BAFU, 2022).

With the increase of farm vehicle weight, subsoils are prone to compaction (Keller et al., 2019). Regardless of the widespread issue, literature on subsoil remediation after compaction is scarce (Berisso et al., 2012; Keller et al., 2017). Subsoils behave differently under compressive forces compared to topsoils (Fu et al., 2019). For example, Wiermann et al. (2000) found a decrease of vertical and round pores upon compaction in the topsoil but not in the subsoil. Hence, insights on compaction and recovery of topsoils cannot simply be transferred to subsoils. In agriculture, subsoil compaction poses a great challenge since it is often invisible under the cover of the topsoil (Johannes et al., 2021b). Reduced water storage and nutrient accessibility due to compaction might only come to light in dry years, when the increased water deficit leads to reduced plant growth (Batey, 2009). On the other hand, soils with compacted subsoils are prone to flooding due to poor water infiltration (Batey and McKenzie, 2006).

Natural restoring mechanisms from compaction in soils are swelling and shrinking, freezing and thawing, bioturbation, and root growth (Dexter, 1991). The structural recovery progression originates from pockets like biopores (Keller et al., 2021). After root decomposition or earthworm passing, a continuous macropore remains in the soil - a biopore is formed. Owing to their high connectivity, biopores improve water and air permeability in soils (Lipiec and Hatano, 2003). However, not all plant species succeed at biopore formation in compacted soils, especially in strongly compacted soil, where soil strength exceeds the growing limit of roots (Cresswell and Kirkegaard, 1995; Gao et al., 2016a).

The most challenging issue of subsoil compaction is the very slow recovery rate after compaction (Schjønning et al., 2015). Natural recovery time scales have been estimated to reach from years to decades, even centuries (Etana et al., 2013; Schjønning et al., 2015). With low biological activity and reduced temperature variations, the natural restoration mechanisms do not work efficiently (Schjønning et al., 2015). Additionally, if penetration resistance is too high, root growth might be limited, which

reduces the formation of biopores (Cresswell and Kirkegaard, 1995). Therefore, it has even been argued that subsoil compaction may be permanent without external aid (Håkansson and Reeder, 1994).

1.3 Mechanical loosening operations

The policy of the Swiss construction supervision of soils (Bodenkundliche Baubegleitung) states that a soil with reduced fertility after constructional work needs to be restored (BAFU, 2022). This is done by mechanical loosening. However, the goal of mechanical operations is not to restore a soil completely but to support the natural recovery mechanisms, which will create suitable physical soil conditions over time (Spoor, 2006). These conditions involve better root penetration, improved aeration, and augmented water infiltration (Hamza and Anderson, 2005). It takes an average ameliorated soil 3-5 vegetation periods to recover fully with the natural restoration mechanisms at work (BAFU, 2022).

Subsoil is loosened with different techniques depending on the degree of compaction and equipment available (Sinnett et al., 2006). In agriculture, the soil is often subsoiled by ripping the soil without turning the soil horizons (Schneider et al., 2017). If the compaction exceeds a certain limit, subsoiling is not possible due to high resistance in soils. In this case, a digger is used, which lifts and drops the soil material separately for each horizon (Sinnett et al., 2006).

Unfortunately, mechanical operations are not always successful (Munkholm et al., 2005; Olesen and Munkholm, 2007; Soane et al., 1987). Even though they have been shown to be effective in topsoils, this is not necessarily the case in subsoils (Spoor, 2006). Since subsoil loosening is very labor- and energy-intensive, an increase in yield due to improved soil conditions is necessary from a monetary and agricultural perspective (Salvador et al., 2009). In a review by Schneider et al. (2017), they found inconsistent results from many studies investigating yield changes after subsoiling. On average, the yield increased by 6 % but 40 % of the studies observed a decrease in yield. Soils with a silty texture (>70 % silt) showed poor results. Mechanical loosening operations were only successful if they lifted a root-inhibiting layer, improved aeration and water availability. Since soil loosening almost completely destroys the inherent pore structure, decreased pore connectivity may lead to poor aeration and reduced water transport in soils (Spoor et al., 2003). Unsuccessful outcomes of mechanical loosening are attributed to reduced water transportation ability. This results in water deficit of roots or, paradoxically, water logging if the water cannot drain from the soil (Schneider et al., 2017; Soane et al., 1987; Spoor et al., 2003).

The long-term success of mechanical loosening also depends on the aftertreatment of the soil (BAFU, 2022). It is advised to omit heavy traffic on an ameliorated soil, especially at moist conditions, since the soil is prone to recompaction due to its weak structure (BAFU, 2022; Munkholm et al., 2005; Schäffer et al., 2007). Additionally, the soil should be cropped with deep-rooting vegetation (BAFU, 2022). Since mechanical loosening is not always a reliable solution, only soils suffering from severe compaction should be mechanically loosened (Munkholm et al., 2005).

1.4 Research question and hypotheses

Whether or not mechanical loosening is a reliable remediation technique is a question that is still under debate in soil science. Few studies have looked at subsoil loosening under very high levels of compaction. Hence, in the course of this master thesis, the following question and hypotheses were investigated:

1. How does mechanical loosening of a heavily compacted subsoil affect physical soil properties and structure?
2. **Hypothesis 1**: Loosening as an ameliorative mechanical operation yields significant improvements regarding physical soil structure and properties compared to compacted soil.
3. **Hypothesis 2**: Within one year, soil structure and properties are not restored completely compared to an uncompacted soil.

To answer this research question, I measured the soil strength with a penetrometer and scanned soil samples with X-rays. Using computer tomography, matrix density and morphological measures were calculated. In the laboratory, the relative diffusivity coefficient and air permeability were measured. Finally, the laboratory measurements and results from the CT images were compared.

Chapter 2

Materials and Methods

2.1 Research site description

The research site of this thesis is located in Switzerland, close to Lake Geneva in Changins and the Jura mountains, 447 meters above sea level. The coordinates are 46°23'53.1" North and 6°13'43.4" East (Swisstopo, 2022). According to WRB taxonomy, the soil is classified as a calcareous Pseudogley with a depth of 71-100 *cm* (Bonnard, 1982). The soil has a loamy texture (Table B.1). Brick fragments were found while sampling the easternmost third of the investigated area. The abundance of brick fragments raises the question of whether classifying the soil of this part of the field as an anthroposol would be more accurate. In the past, the field was used for other agricultural experiments carried out by Agroscope (pers. com. Alice Johannes, 2022). The detailed descriptions of these experiments were not available.

2.2 ROCSUB project

This thesis is part of the ROCSUB project, which stands for *restoration of a severely compacted subsoil*. During construction works of the new AO building on the Agroscope ground at Changins, the field of the project served as a deposit of excavation material for several years until 2019 (Figure 2.1a). The responsible construction company removed the topsoil before the pile of soil material was stacked on the field. The highest point of the deposit reached approximately ten meters in height (Figure 2.1b). The long-standing overlying pressure of the pile resulted in a high degree of subsoil compaction.

After the construction work was finished, the company removed the deposit and returned the topsoil to its original place. Later, the construction supervision of soils (Bodenkundliche Baubegleitung) discovered the strong compaction of the subsoil. Together, the construction company, the construction supervision of soils, the Federal Office for the Environment (BAFU), and the Agroscope initiated the ROCSUB project.

(A) Areal photo of the research site from 2015 with the deposit in the lower left (Johannes et al., 2021a).

(B) Side view of the deposit. The white arrow indicates the previously removed topsoil (Johannes et al., 2021a).

FIGURE 2.1: Top and side view of the construction material deposit.

In 2020, the uncompacted topsoil was removed to loosen the underlying subsoil mechanically. Due to the high levels of compaction, subsoiling was impossible. Hence, a digger had to lift and drop the soil material to induce cracks in the dense material. Only two stripes of nine meters in width were mechanically loosened, and the remaining area was left compacted and unchanged (Figure 2.2). Immediately after applying the topsoil on the loosened subsoil, grassland was planted to prevent erosion and recompaction.

(A) Mechanical loosening of the soil with a digger (Photo: Alice Johannes).

(B) Mechanical loosening in two stripes of the field (Photo: Alice Johannes).

FIGURE 2.2: Mechanical loosening of the compacted soil in 2020.

Over six years, the changes in subsoil structure recovery will be monitored and analyzed. The soil was covered in grass when the soil samples were taken in April 2021. In the middle of the field, as a line pointing in the North-Eastern direction (Figure 2.4), salix trees were planted a month before the sampling took place. However, the influence of salix roots on soil structure recovery is not part of this thesis since the tree roots most likely had no measurable effect on the sampled soil structure within a month.

Since the previously removed topsoil was stored next to the pile of construction material, the soil close to the compacted site also showed signs of moderate compaction. Therefore, the reference plot, where it was assumed that no compaction had occurred, was chosen at 40 meters from the compacted site (Figure 2.3).

2.3 Sampling strategy

In January 2020, premeasurements with a penetrologger were conducted by Alice Johannes to quantify the degrees of compaction on the research site. Since the soil had not been compacted purposefully, the compaction levels differed strongly horizontally and vertically. A clearer picture arose by smoothing the spatial pattern and adding a median filter (Figure 2.3). Nevertheless, the degrees of compaction remained spatially highly variable. In the center of the field, an area of relatively homogeneous compaction degree was detected. This area was chosen as the sampling location (Figure 2.4).

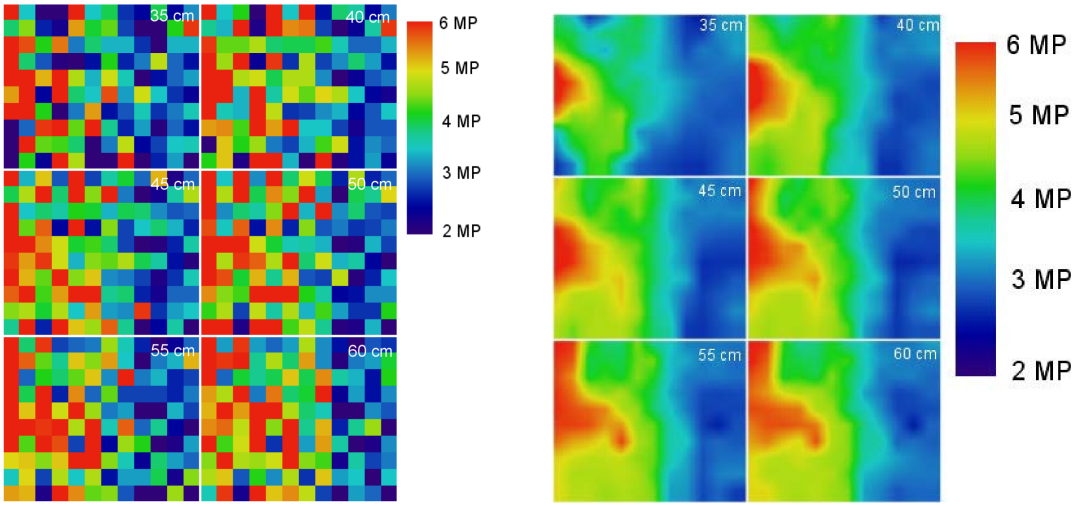

(A) Penetrologger measurements showed for different depths (35-60 cm) (Johannes et al., 2021a).

(B) Penetrologger measurements smoothed with a median filter for different depths (35-60 cm) (Johannes et al., 2021a).

FIGURE 2.3: Penetrologger measurements as heatmap.

The core samples were taken in April 2021 with an Eijkelkamp sample ring kit and stored in aluminum cylinders (Eijkelkamp, 2019). The aluminum cylinders were 0.05 m high with a diameter of 0.05 m and a volume of 100 cm^3. Due to an arid spring, the topsoil was dry. The subsoil was moderately moist. Soil samples were taken from 10 cm (topsoil), 30 cm (upper subsoil), and 60 cm (lower subsoil) depth in the *compacted*, *loosened*, and *uncompacted* treatment (Figure 2.4). The *uncompacted* treatment corresponds to the reference plots described in chapter 2.2. A total of 135 samples were taken, 15 in each depth and treatment. Due to the dry conditions, three

FIGURE 2.4: Sampling location and field classification in *compacted*, *loosened*, and *uncompacted* plots (Johannes et al., 2021a).

topsoil samples were of overly poor quality and discarded. Therefore, the analysis was conducted with 132 core samples.

2.4 Penetrometer

Prior to any mechanical improvements to the soil structure, the penetration resistance was measured by Alice Johannes on 22^{th} January 2020 (Figure 2.3). The measurements were conducted after a precipitation event of 10 *mm* three days earlier (Meteotest, 2022). The matric potential was -25 *hPa* at 30 *cm* and -51 *hPa* at 60 *cm* depth (Table B.2). The measurement station is not located precisely on the ROCSUB field but at a distance of 590 *m* to the field. Indeed, the subsoil at the measurement station is not equally compacted as on the ROCSUB field. The matric potential values are only supposed to estimate the water saturation. The instrument used was an Eijkelkamp Penetro Viewer Vs. 6.08 with a cone area of 1 cm^2 (Eijkelkamp, 2018b), which measures the penetration resistance automatically and includes depth. The maximum sampling depth was 80 *cm*, but since 80 *cm* was rarely reached, only the first 60 *cm* were considered.

The second measurement for the penetration resistance was conducted on 4^{th} November 2021 after 73 *mm* of rainfall during the five days prior to the measurement (Meteotest, 2022). The second measurement of the penetration resistance was done under moister conditions than the previous measurement in January 2020. -13 *hPa* (30 *cm* depth) and -10 *hPa* (60 *cm* depth) matric potential were measured (Table B.2). Additionally, soil moisture was measured with a frequency domain reflectometry (FDR) instrument installed on the ROCSUB field at depths of 15 *cm*, 35 *cm*, and 60

cm in the three treatments. Since the FDR was installed in April 2021, there is no data from January 2020.

Instead of a penetrologger, an Eijkelkamp hand penetrometer Vs. 6.01 with a cone area of 1 cm^2 was used (Eijkelkamp, 2018a). Contrary to the penetrologger, the penetrometer only displays the penetration resistance every 10 *cm* that needs to be noted manually. Measurements were made to a depth of 60 *cm*. The measurement unit was *Newton* and was later converted to *Megapascal*. In the plots cropped with salix, the distance of the penetration point to each plant was 20 *cm*.

2.5 X-ray tomography

Soil samples were scanned at the ETH in Zurich with an X-ray scanner GE phoenix v | tome | x s 240 featuring a GE DXR250 HCD (4MP) detector plate with 2024 x 2024 crystals in x and y directions (GE Sensing Inspection Technologies GmbH, Wunstorf, Germany). At the time of the X-ray measurements, all soil samples had a consistent matrix potential of -100 *cm*. Before the measurements, the detector plate was calibrated to prepare the scanner. To limit image noise, the binning was used and set to 2x2 pixels. Several optical filters were applied (two of 0.1 *mm* copper and one of 0.5 *mm* copper) to filter photons of low energies and avoid beam hardening. The X-ray tube was operated with an electron flow of 420 μA with a voltage of 150 kV. The voxel size was 63.216 μm. The resulting resolution corresponds to the minimal distance at which two objects can be distinguished and is approximated as twice the voxel size (126 μm). The scanning time per sample was 7 minutes. A 16-Bit unsigned grayscale was chosen for the image reconstruction to keep the file size within reasonable limits (4 GB). The gray values reach from 0 (black) to 65 536 (white) in an unsigned 16-Bit image.

Twenty-six samples were scanned in October 2021. Since the X-ray scanner broke down, the remaining 106 samples were scanned five months later, in February 2022 when the scanner was operational again. During the five months, the samples were covered with a lid on both sides and stored in a box at 7 °C to limit water evaporation.

2.6 Image processing

For image processing, the Fiji ImageJ software was used (Schindelin et al., 2012). If not stated otherwise, the following steps were conducted using the plugin SoilJ version 1.2.18 for image processing (Koestel, 2018). Additional macros written for this thesis are listed in the Appendix C. The images obtained from the X-ray scanner were in raw format. These files were converted to tiff format using a macro in the first step (see Appendix C.1). The resulting images were straightened and centered

with the SoilJ plugin. In the next step, the wall coordinates, top and bottom of the column, were identified with SoilJ. However, some images had to be resliced manually since the detection did not go smoothly. A 3D adaptive Gaussian filter was applied with a 2x2x2 kernel size to remove noise from the image (Ollion et al., 2013) (see Appendix C.2).

Image processing aims to classify voxels according to different materials in the soil: air-filled pores, particulate organic matter (POM) and roots, and soil matrix. This process is called segmentation. Particulate organic matter consists of bits of plant tissue (Weil and Brady, 2017). In subsoils, most organic carbon stems from plant roots (Rumpel and Kögel-Knabner, 2011). In the CT images, fresh roots are included in POM as well. Since materials differ in density, they also differ in gray values. The denser the material is, the brighter the gray value. For example, specific ranges of dark gray values are identified as air-filled pores. However, deciding where to set the shared threshold over all 132 images for each material is non-trivial. There are standardized procedures that work with the histogram of the gray values. For example, the minimum method sorts the materials according to the minimum between two peaks. However, due to the strong compaction, there were very few air voxels in the 3D images. Therefore, the air peak was shallow, and the standardized minimum method was very unreliable (Figure 2.5).

In this case, the threshold needs to be selected manually by comparing the performance of the chosen threshold between the images and adjust it until it includes all the gray values of interest (e.g. air-filled pores). This procedure only works correctly if all 16-Bit images are calibrated at the same grayscale. If the calibration was successful, identical materials exhibit the same gray values throughout all the images. The calibration used the following formula:

$$x = \frac{(s - l) \cdot (T_u - T_l)}{(u - l)} + T_l \tag{2.1}$$

s is the current gray value of the voxel and x the gray value after the calibration. The SoilJ plugin needs an upper and lower reference gray value to recalculate the gray value of each voxel relatively to the reference values. The target variables describe the reference value to which the gray value of the image is adjusted. T_l is the lower reference target value and T_u the upper reference target value. These are equal for all 132 images. For T_l, a gray value of 5000 was chosen, representing air-filled pores. The upper target value T_u was set to a gray value of 20 000, representing the value of the column material aluminum. The u and l mark the sampled gray value from each image, respectively. Therefore, u and l are different for each 3D image.

Under normal circumstances, the reference value for air (l) is chosen in an air-filled

pore within the column. However, a third of the samples showed severe compaction, offering too few pores to sample within the column. On the first try, the lower reference value was taken closely outside the column by the algorithm of SoilJ. For comparison, an additional reference value sampling was performed far away from the cylinder wall. However, both resulting calibrations were of poor quality, showing high variability in the gray values of air and POM between different images.

Therefore, a second calibration was done using a Python 3.9 script (see Appendix C.3). For the lower reference value (l), the median of two manually selected air voxels of three different 2D image slices in each 3D image was taken, making it a total of six sampled values per 3D image. From the six values, the median was calculated and used as the lower reference value (l). The upper reference value was left unchanged since the gray values of the aluminum wall were all approximately at 20 000 after the initial calibration attempt and did not show high variability. In the next step, the histogram of the gray values in each of the 132 3D images was extracted and further processed using Python 3.9.

A 1D median filter with a window size of ten was applied to smooth each image's histogram individually. In the next step, the mean over all 132 histograms was calculated. The resulting mean histogram was smoothed using a 1D median filter with a window size of 50. In Figure 2.5 the 1D filtered histogram over all 132 3D images is shown. The peak of the histogram is called the mode. The y-axis marks the frequency (abundance of voxels), and the x-axis the gray values. The small peak at the gray value of 5000 marks the air-filled pores, and the large peak between 15 000 and 20 000 shows the gray values of the soil matrix. These voxels contain a combination of air-filled pores, water-filled pores, and solid material (Lamandé et al., 2013). The pores in these voxels are smaller than the image's resolution.
The threshold was identified manually, comparing its feasibility to every single histogram. A gray value of 12 000 was selected as the threshold below which the voxels are classified as either air-filled or POM. Additionally, the gray value of 8000 was chosen as the best threshold between air-filled pores and POM.

The images were segmented with SoilJ according to the two thresholds. This resulted in a binary image with white voxels classified as pores and a second binary image with white voxels classified as pores and POM. The pore images were subtracted from the pore and POM image to extract only the POM voxels. After the subtraction, partial volumes were removed by eroding and dilating (morphological opening) the images once three-dimensionally on the white voxels. The resulting image contained only POM voxels displayed in white.

In a further step, the pore space analyzer in SoilJ was run. The pore space analyzer evaluates the morphological properties in a binary image with the help of the

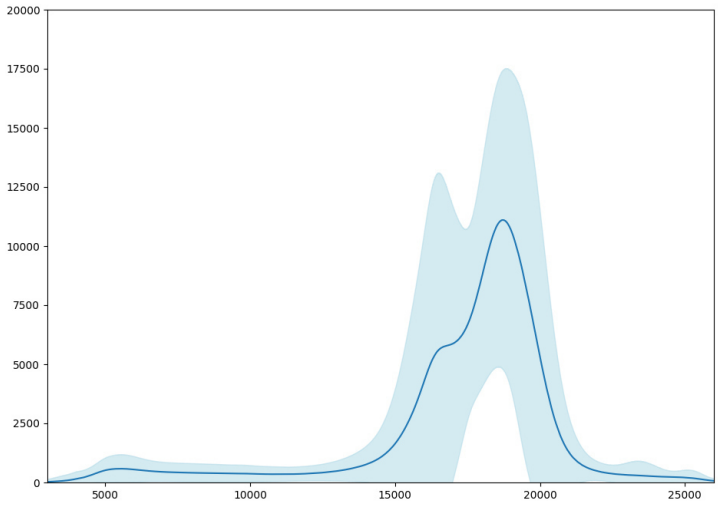

FIGURE 2.5: Mean histogram with standard deviation of all 3D images.

BoneJ plugin (Doube et al., 2010). It calculates the following morphological measures: macropores volume, average thickness, bottleneck diameter, cluster thickness, and percolation. These measures extracted macroporosity, pore size distribution, average pore diameter, bottleneck diameter, and percolating properties. Percolating samples offer an imaged pore connection from top to bottom. The percolation threshold is the theoretical porosity at which a percolating cluster would emerge (Soto-Gómez et al., 2020). The ratio of the percolating pore volume to the total pore volume is called the percolating volume fraction. The bottleneck diameter marks the diameter of the largest sphere that could be moved through the pore network from top to bottom.

Since scanning artifacts resulted in a brightness shift in the bottom and top of the soil columns, 70 voxels were removed on both sides. Since the soil material detached from the cylinder wall in some samples, this could influence the measurement of the pore properties. The pore space analyzer was run for the pore voxels, with 60 voxels cut from the wall to ensure a more representative volume. SoilJ is capable of differentiating biopores and non-biopores according to their pore shape. Biopore analysis and POM segmentation resulted both in additional binary images, on which the pore space analyzer was run.

The samples scanned in October 2021 were reconstructed with the GE beam-hardening correction. However, this was not done for the samples scanned in February 2022, which led to brighter gray values in the images scanned in February compared to those scanned in October. Hence, the histogram analysis of matrix density was conducted only with the 113 samples scanned in February (chapter 3.3). Omitting the

samples scanned in October led to a reduced sample size. However, the omitted samples were almost from all depths and treatments, which did not result in a very uneven sampling size. The smallest number of samples per treatment and depth was 11 samples. Before publication, the image analysis of this thesis should be repeated with uniformly reconstructed images by the ROCSUB scientists.

2.7 Air diffusion and air permeability

Diffusion and air permeability were measured at -30 hPa, -100 hPa, and -300 hPa matric potential by Marlies Sommer in the soil physics laboratory at Agroscope. The air permeability measurements were conducted with a prototype device (Agroscope, 2018). Air is pushed through the soil sample. The device measures how much air must be pushed through until 2 hPa resistance is reached. Air permeability measurements below the measurement threshold of $<$2.3 μm^2 were set to 2.3 μm^2 and considered impermeable.

The relative gas diffusivity coefficient $\left[\frac{D_p}{D_o}\right]$ was measured with a prototype device (Agroscope, 2019). The top of the soil sample is placed in a chamber, shut air-tight, and filled with nitrogen gas. The bottom of the soil sample is exposed to the surrounding air. Over 45 minutes, the oxygen concentration is measured as it slowly diffuses back into the chamber through the soil sample. From here on, the relative gas diffusivity coefficient will be referred to as air diffusion.

If the measured diffusion values were slightly below zero, they were set to zero. Negative diffusion values were very close to zero and lay within the fluctuation of the measurement device. For some samples, the measured diffusion value at -100 hPa was higher than that at -300 hPa. This is not realistic since smaller pore diameters are drained at -300 hPa and the diffusion is supposed to increase when more pores are drained. The values with this behavior were manually removed. Additionally, at -300 hPa, the laboratory assistant detected a visible detachment of the soil matrix from the aluminum cylinder. Since the gap between the soil matrix and the cylinder significantly influences the diffusion and air permeability measurements, these samples were removed as well.

2.8 Capillary rise

To compare measured values at different moisture levels, it is important to know which pore diameters are drained and which diameters are still occupied by water. The formula of the capillary rise enables this calculation:

$$h = \frac{4\sigma cos\alpha}{\rho g d} \tag{2.2}$$

where σ is the surface tension of water, α the contact angle, ρ the density of water, g the gravitational acceleration, and d the diameter of the tube. In this idealized formula, the pores are approximated as tubes of diameter d, where the water rises as high as the diameter allows. At room temperature, σ is assumed to be 0.0728 $\frac{J}{m}$, α is assumed to be 0°, ρ is 1000 $\frac{kg}{m^3}$, and g is 9.81 $\frac{m}{s^2}$ (Hendriks, 2010). With these values, the formula is simply:

$$h \approx \frac{2.8 \cdot 10^{-5} m^2}{d} \tag{2.3}$$

Since the matric potential [hPa] is equal to the negative pressure head [m], the following table is deduced:

TABLE 2.1: Drained pore diameter at specific matric potential Ψ according to equation 2.3.

Ψ [hPa]	**d** [μm]
-30	>93.2
-100	>28.0
-300	>9.3

The matric potential of -100 hPa marks the field capacity, which is the maximum amount of water the soil can hold against gravity (Hendriks, 2010). Usually, the drained pores at the field capacity are referred to as macropores (>30 μm diameter) (Hendriks, 2010). However, in this thesis, macropores are defined as pores with diameter >126 μm since these are the smallest pores visible in the X-ray images with the given resolution.

2.9 Statistics

The data analysis was conducted with Python 3.9. Since depth is an influencing variable, only treatments within the same depth were compared. When comparing different depths, only one treatment was analyzed. First, the data was checked for normal distribution using a Shapiro Wilkinson test. If the data was not normally distributed, they were transformed logarithmically or by taking the square root.

Furthermore the data was analyzed for homoscedasticity with a Bartlett's test for normally distributed data and Levene's test for non-normally distributed data to check the data for equal variance. If the normal distribution was not reached and the variance was unequal, a Kruskal Wallis test for non-normally distributed data was conducted to test the data for significant differences. If the data was normally distributed and homoscedastic, an ordinary least square (OLS) model was fitted using Python. To assess the reliability of the OLS model, the residuals were checked for normal distribution. If the data was heteroscedastic but normally distributed, a weighted least square (WLS) regression model was applied with the inverse of the

variance as weight. To enhance the contrast and test the data for variance difference between the treatments, a posthoc test was applied (Tukey test). The same test was used to compare the histograms since this test works as well for unequal sample sizes. As a significant p-value, 0.05 was taken.

Chapter 3

Results

3.1 Penetration resistance

In the measurements conducted by Alice Johannes in January 2020, the soil was not yet loosened (Figure 3.1a). There was no significant difference in soil strength between the treatments in the topsoil. The penetration resistance increased with depth except for the *uncompacted* treatment. In the subsoil, the penetration resistance in the *uncompacted* treatment differed significantly from the values in the *compacted* and *before loosened* treatments (p-values: <0.05). The soil strength at 30 *cm* depth of the *before loosened* treatment did not differ from the soil strength in the *compacted* treatment (p-value: 0.14).

In the topsoil, the penetration resistance between the treatments did not differ in the measurements conducted in November 2021 (Figure 3.1b). The soil strength of the *compacted* treatment showed the highest and most variable penetration resistance at 30 and 60 *cm* depth (p-values: <0.01). The lowest penetration resistance was observed in the *loosened* plots (p-values: <0.01). Soil strength increased with depth (p-values: <0.01), except for the *loosened* treatment (p-value: 0.14). The penetration resistance measured in January 2020 was significantly higher compared to the measurements from November 2021.

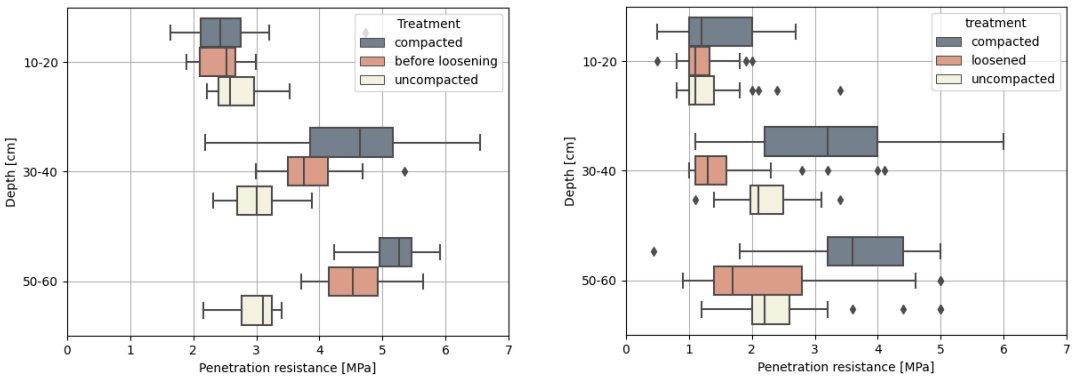

(A) Penetrologger measurements in January 2020 (before loosening).

(B) Penetrometer measurements in November 2021 (after loosening).

FIGURE 3.1: Penetration resistance [*MPa*].

3.2 Visual results of CT images

In Figure 3.2, samples from different treatments are shown from above. The *compacted* sample shows little pores and a dense soil matrix (Figure 3.2a). More macropores are visible in the *loosened* samples (Figure 3.2b). In the *uncompacted* sample, the macropores have a rounder shape (biopores) than in the *loosened* sample (green circle) (Figure 3.2c). Close to the center of the *uncompacted* sample, in lighter gray values than the pores, a root is shown (red square).

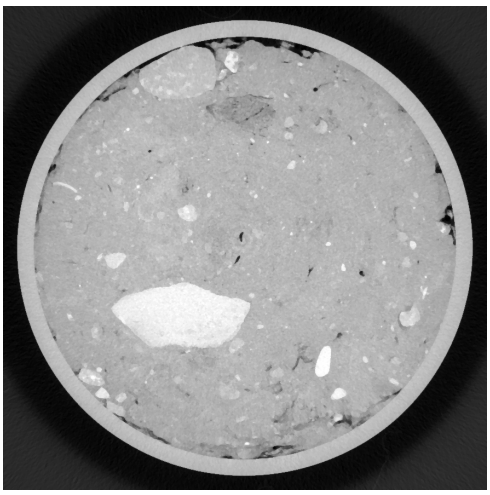

(A) compacted.

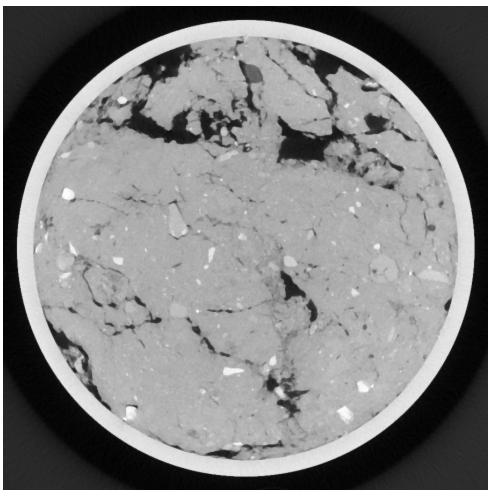

(B) loosened.

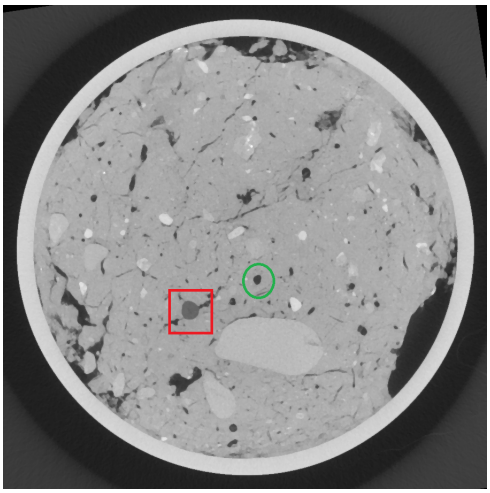

(C) uncompacted.

FIGURE 3.2: Top view of X-ray scanned samples from 30 *cm* sampling depth. Roots are marked in a red square and a biopore in a green circle.

The *compacted* sample does not show visible macropores from the side view either (Figure 3.3a). In the *loosened* sample, remaining fragments from the loosening operation are clearly visible and marked in red (Figure 3.3b). Round biopores are also visible from the side in the *uncompacted* treatment and were marked in green (Figure 3.3c).

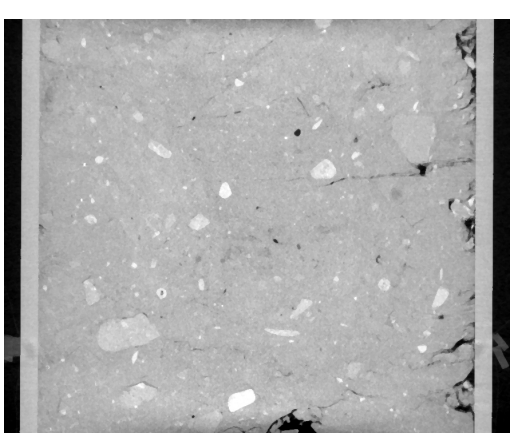

(A) compacted.

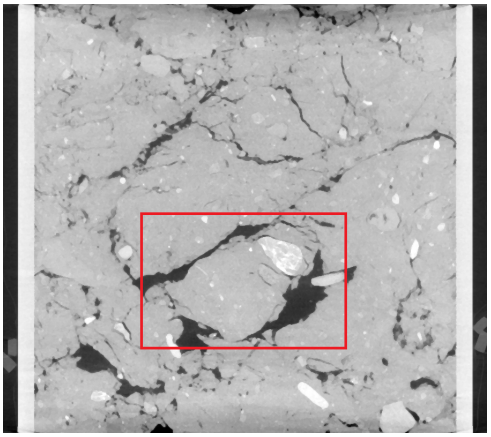

(B) loosened.

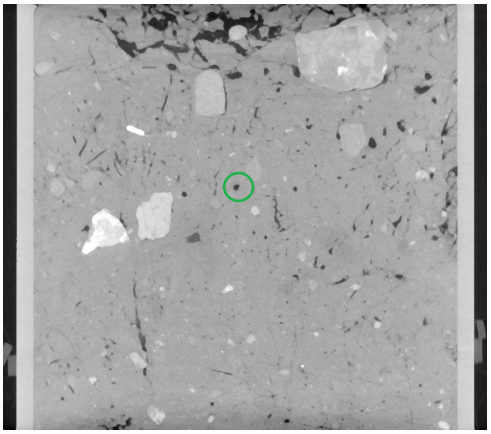

(C) uncompacted.

FIGURE 3.3: Side view of X-ray scanned samples (30 *cm* sampling depth) with a biopore marked in a green cicle in the *uncompacted* sample and a fragment marked in red in the *loosened* sample.

Red pore clusters mark the percolating macropores, which have a visible connection from the top of the sample to the bottom (Figure 3.4). In the *compacted* sample, there was no percolating cluster and very few pores (Figure 3.4a). In the *compacted* treatment, samples were rarely percolating. An example for a *compacted* sample with a percolating pore cluster is Figure 3.4b, where a crack in the soil matrix formed a connected pore. The *loosened* treatment showed much more pores than the *compacted* treatment. However, the pore clusters were not well connected since no cluster was marked in red (Figure 3.4c). In the *uncompacted* sample, a percolating pore cluster emerged. In comparison to the *loosened* sample, the *uncompacted* sample showed a better connected pore space with more tube-like clusters (biopores) (Figure 3.4d).

(A) compacted I.

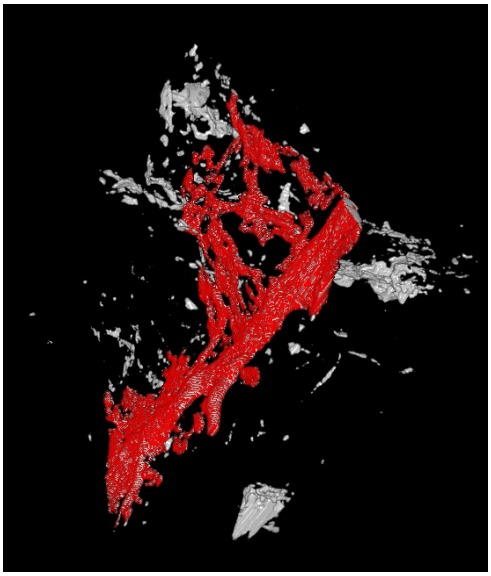

(B) compacted II.

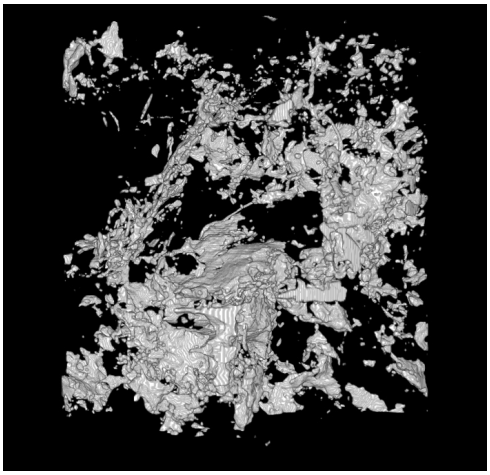

(C) loosened.

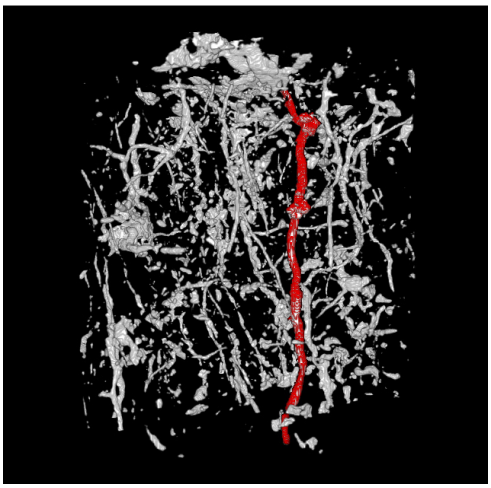

(D) uncompacted.

FIGURE 3.4: 3D visualization of pore space with percolating pore clusters marked in red from 30 *cm* sampling depth.

3.3 Histograms from 3D images

The histograms in Figure 3.5 were cropped to the gray values of interest (15 000 - 22 000), which contain the soil matrix. In the interval of the soil matrix, the histograms followed a normal distribution. With increasing sampling depth, the modes of the histograms moved to higher gray values. Additionally, the modes move further apart from top to subsoil.

The distribution of the histograms in the topsoil was flat (Figure 3.5a) which indicated a high variance. In the subsoil, the distribution of the histograms became steeper (Figures 3.5b and 3.5c). Hence, the variance was smaller, but the histogram of the *loosened* treatment still showed high variability. In the topsoil and the upper subsoil, the histograms did not differ significantly between the treatments (p-values: >0.12). In the lower subsoil, the mode of the *uncompacted* treatment showed the lowest value (p-value: <0.01), followed by the mode of the *loosened* treatment. The mode of the *compacted* treatment was highest (p-value: <0.01).

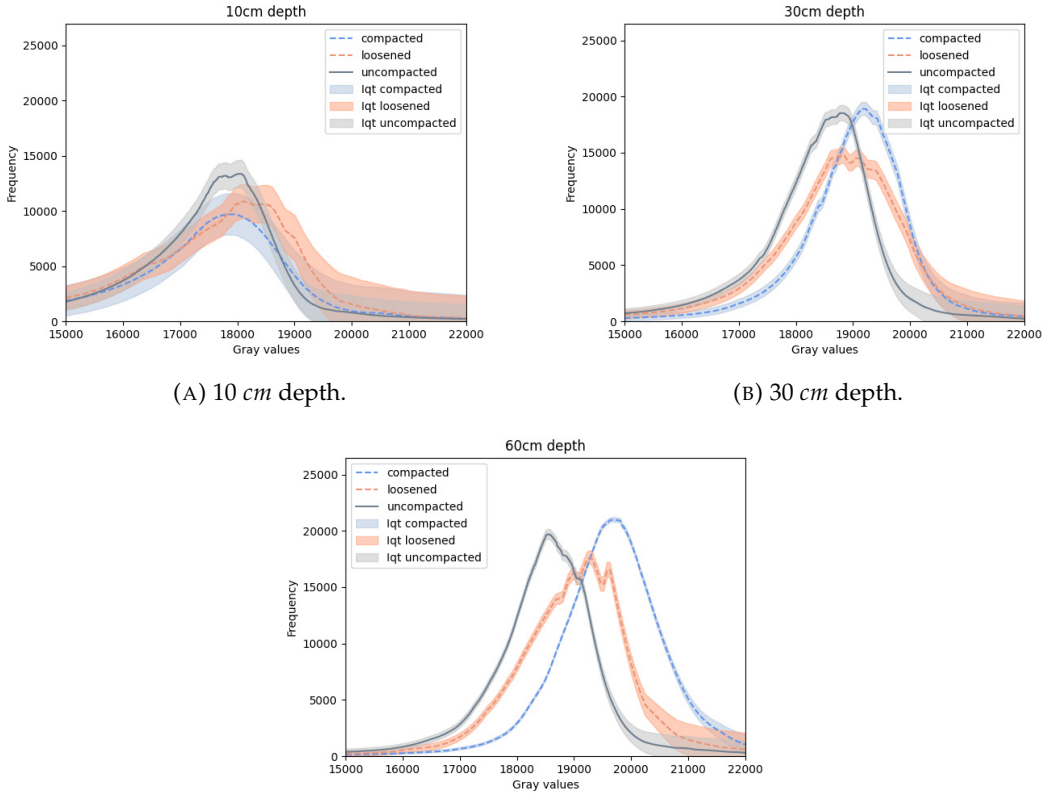

(A) 10 *cm* depth.

(B) 30 *cm* depth.

(C) 60 *cm* depth.

FIGURE 3.5: Median histograms of the different treatments with interquartile range (iqr) smoothed with a 1D median filter of window size 100.

3.4 Macroporosity

In the topsoil, the visible macroporosity (for pores >126 μm diameter) was very variable (Figure 3.6). The macroporosity of the *loosened* treatment was lower compared to the value of the *compacted* treatment (p-value: 0.03).
At 30 *cm* depth, the macroporosity did not differ significantly between treatments. Further down at 60 *cm* depth, the macropores were nearly entirely absent in the *compacted* treatment. In comparison to the *compacted* treatment, there were more macropores in the *loosened* treatment (p-value: 0.04) but not in the *uncompacted* treatment (p-value: 0.13). With increasing depth, the *loosened* treatment was the only treatment with a not significantly different macroporosity (p-value: 0.66).

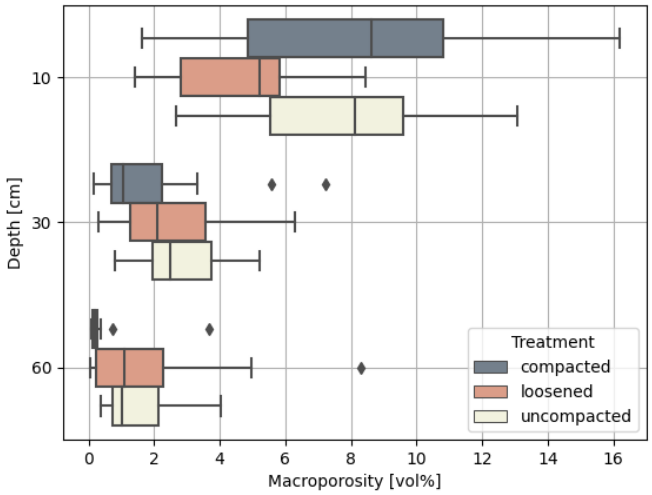

FIGURE 3.6: Visible macroporosity (>126 μm diameter) [$vol\%$] in the different treatments in depths of 10 *cm*, 30 *cm*, 60 *cm*.

3.5 Pore size distribution and average pore diameter

The average pore diameter (>126 μm) did not change strongly with sampling depth (Figure 3.7). In the topsoil, the average pore diameter of the *uncompacted* treatment was significantly higher than the value of the *loosened* and *compacted* treatment (p-values: 0.03). In the subsoil, the difference in average pore diameter between the treatments was insignificant (p-value: >0.65). The only treatment that showed a significant decrease in average pore diameter with depth was the *uncompacted* treatment (p-value: 0.05).

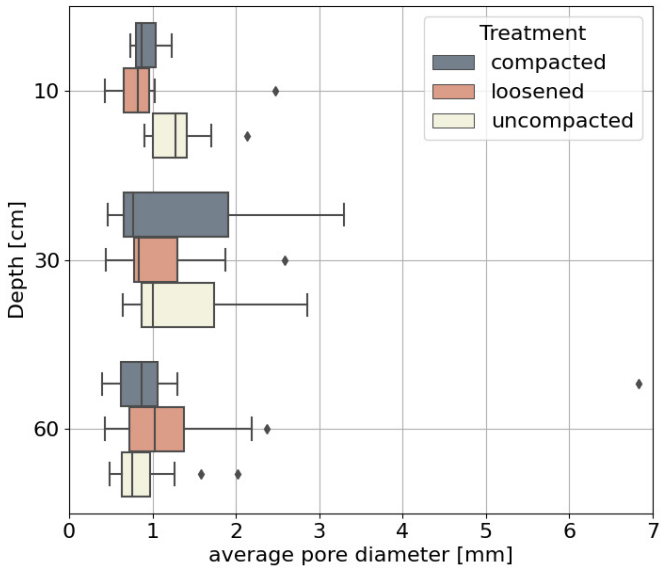

FIGURE 3.7: Average pore diameter (>126 μm) [mm] in the different treatments in depths of 10 cm, 30 cm, 60 cm.

The macropore volume decreased with depth in all pore diameters (Figure 3.8). In the topsoil, the *uncompacted* treatment had the most evenly distributed macropore diameter (Figure 3.8a). In contrast, the macropore diameter of the *loosened* treatment was very unevenly distributed, showing a high pore volume in small macropores (<0.5 mm) and a low volume of large macropores (>1.2 mm). The *compacted* treatment had the highest volume of small macropores in the topsoil.

In the subsoil, the *compacted* treatment showed the lowest volume of macropores throughout the different diameter classes in the subsoil (Figure 3.8b and 3.8c). As in topsoil, the *uncompacted* treatment showed the most even distribution. The *loosened* treatment was more unevenly distributed, showing low volume at large pore diameters and high volume at small pore diameters.

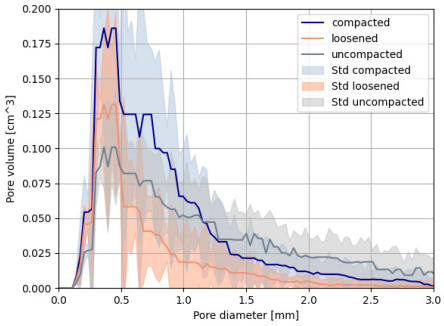

(A) 10 *cm* depth.

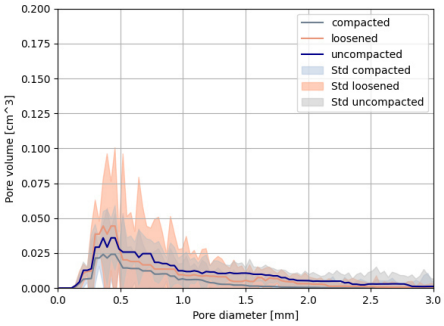

(B) 30 *cm* depth.

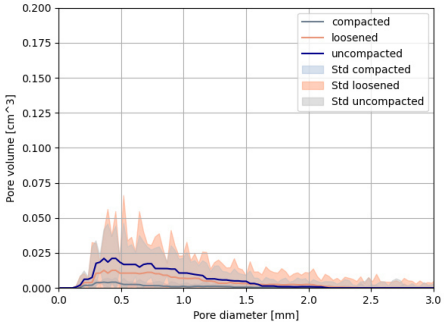

(C) 60 *cm* depth.

FIGURE 3.8: Macropore size distribution from 0.126 - 3 *mm* in pore volume [cm^3].

3.6 Percolation

The percolating volume fraction (for pores >126 μm diameter) showed a higher variability in the topsoil (Figure 3.9a). Both *compacted* and *uncompacted* treatments showed a high percolating volume fraction, whereas in the *loosened* treatment mostly no percolating pore cluster was found for the imaged pores (p-values: 0.03). In the subsoil, the percolating fraction became very small, and only the *uncompacted* treatment showed a value above the resolution.

Figure 3.9b displays the percentage of percolating samples. In the topsoil, samples from the *compacted* and *uncompacted* treatment percolated more often compared to those from the *loosened* treatment. In the *uncompacted* treatment, many samples had a connecting pore space from top to bottom throughout the sampling depths. However, in the *compacted* and *loosened* treatment, fewer samples were percolating, especially in the subsoil.

The median percolation threshold in the *uncompacted* treatment in the subsoil was very low compared to the percolation threshold of the other treatments (p-value:

<0.07) (Figure 3.9c). The *compacted* treatment showed the highest percolation threshold in the subsoil. In the top and upper subsoil, the difference between the treatments was not significant except for the difference between *compacted* and *uncompacted* treatment (p-value: <0.01). However, in the lower subsoil, all treatments differed significantly (p-value: <0.01).

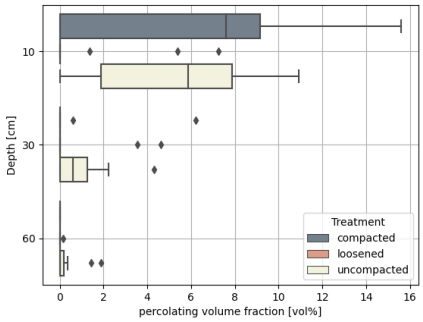

(A) Ratio of percolating pore volume to total pore volume (>126 μm diameter) [$vol\%$] in the different treatments in depths of 10 cm, 30 cm, 60 cm.

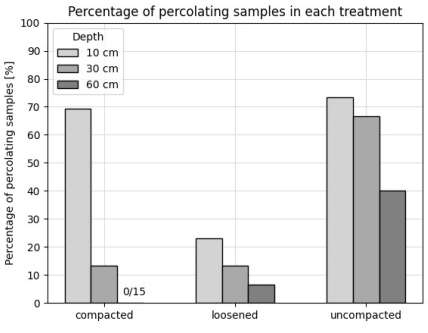

(B) Percentage of percolating samples [%] in the different treatments in depths of 10 cm, 30 cm, 60 cm.

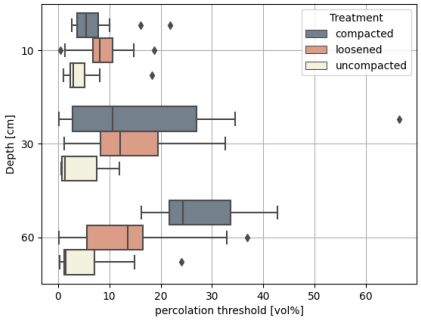

(C) Percolation threshold (>126 μm diameter) [$vol\%$] in the different treatments in depths of 10 cm, 30 cm, 60 cm.

FIGURE 3.9: Percolation properties.

3.7 Bottleneck diameter

In the topsoil, the *uncompacted* treatment showed the largest median bottleneck diameter (>126 μm) (Figure 3.10). The bottleneck diameter of the *uncompacted* treatment differed significantly from the values of the other treatments (p-value: 0.05). The smallest median bottleneck diameter was observed in the *loosened* treatment. In the subsoil, only the *uncompacted* treatment had a median bottleneck diameter above the image resolution. The decrease of the bottleneck diameter with depth in the *uncompacted* treatment was only significant for the upper to lower subsoil (p-value: <0.01).

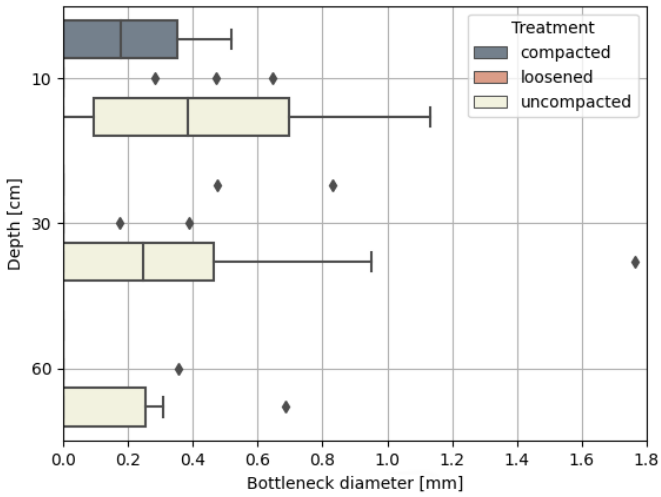

FIGURE 3.10: Bottleneck diameter (>126 μm diameter) [mm], which visibly connects the top and bottom of the soil column.

3.8 Biopore ratio

In Figure 3.11 the median ratio of biopores to non-biopores is shown. A high median biopore ratio indicates an abundance of biopores compared to non-biopores. More biopores were found throughout the profile in the *uncompacted* treatment (p-value: <0.01). Additionally, the median biopore ratio increased with depth (p-values: 0.09 and <0.01). No difference was found between the ratio of the *loosened* and *compacted* treatment in the subsoil at 30 cm (p-value: 0.30) nor at 60 cm (p-value: 0.21).

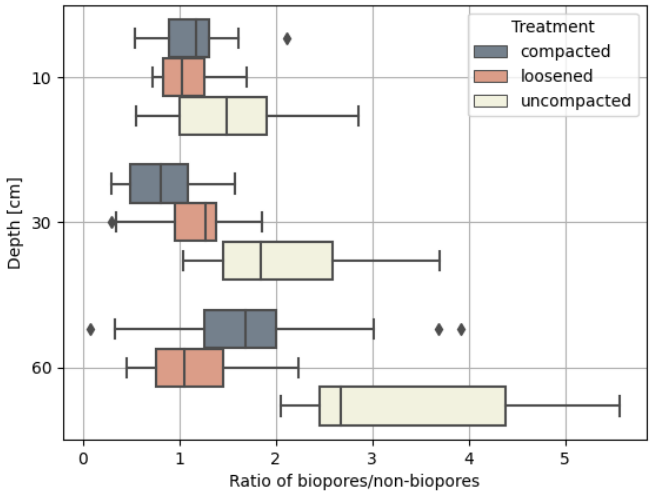

FIGURE 3.11: Fraction of percolating pores (>126 μm diameter) in the different treatments in depths of 10 cm, 30 cm, 60 cm.

3.9 Particulate organic matter (POM) and roots

The POM content marks the ratio of POM and roots to the total volume of the soil sample (with 60 voxels removed from the wall) (Figure 3.12). The topsoil's highest variability and POM content was found in the *compacted* treatment. The *uncompacted* treatment showed a significantly lower POM content in comparison to the *loosened* (p-value: <0.01) and *compacted* treatments (p-value: <0.01). From the topsoil to the subsoil, there was a strong decrease in POM content in all treatments (p-value: <0.05). At 30 *cm* depth, there was no significant difference in the POM content between the treatments (p-values: >0.44). In the lower subsoil (60 *cm*), there was nearly no POM content observed in the *compacted* treatment compared to the value in the other treatments (p-values: <0.01). The POM content of the *uncompacted* and *loosened* treatment did not differ significantly at 60 *cm* depth (p-value: 0.88).

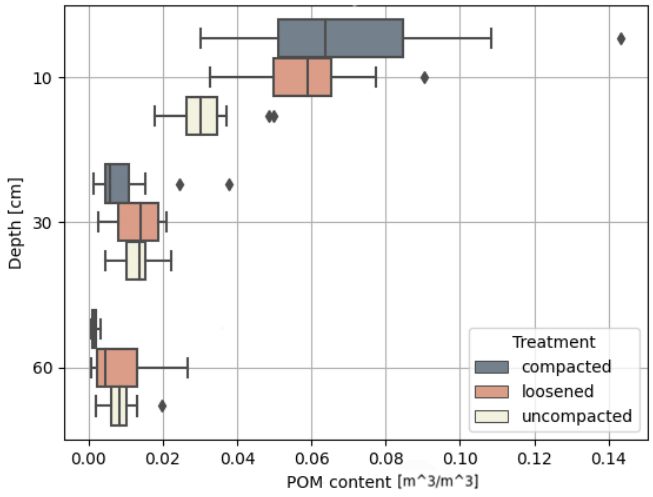

FIGURE 3.12: Particulate organic matter (POM)-content [%] in the different treatments in depths of 10 *cm*, 30 *cm*, 60 *cm*.

3.10 Air diffusion

With drier conditions, the air diffusion increased (Figure 3.13). At -30 *hPa* matric potential, a higher variability was observed in the topsoil (Figure 3.13a). The treatments did not differ significantly in each depth (p-value: >0.25).

At -100 *hPa*, the air diffusion of the topsoil did not differ significantly between the treatments (p-values: >0.40) (Figure 3.13b). At 30 *cm* depth, the air diffusion of the *uncompacted* treatment showed the highest air diffusion. A similar tendency was observed at 60 *cm* depth, where the diffusion of the *uncompacted* treatment was insignificantly higher (p-value: 0.07). The air diffusion of each treatment showed a

decreasing diffusion from top- to subsoil (p-values: <0.01) but not within the subsoil (p-values: >0.12).

At -300 *hPa*, there was no significant difference in topsoil diffusion between the treatments (Figure 3.13c). In the upper subsoil (30 *cm*), the *compacted* treatment showed a significantly lower diffusion compared to the value of the other treatments (p-values: 0.04). In the lower subsoil (60 *cm*), the air diffusion of the *loosened* treatment was higher than the value of the *compacted* treatment (p-value: 0.02) but did not differ significantly from the *uncompacted* treatment (p-value: 0.11).

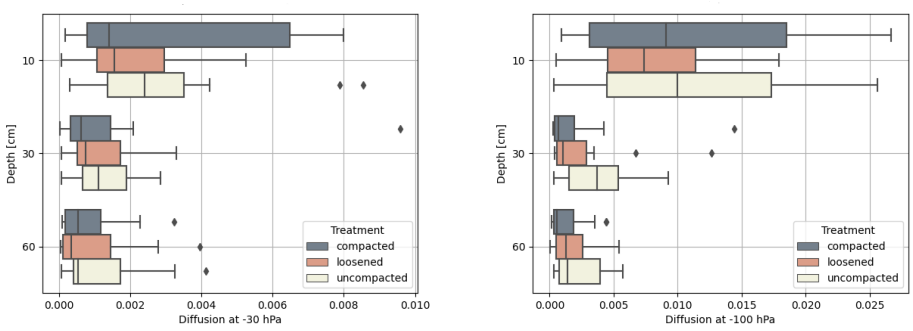

(A) -30 *hPa*. (B) -100 *hPa*.

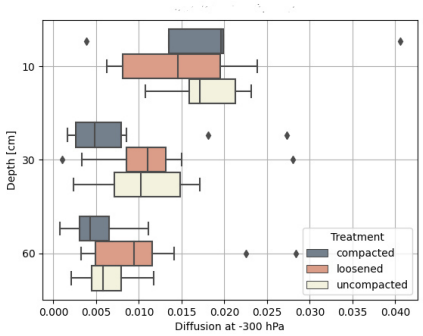

(C) -300 *hPa*.

FIGURE 3.13: Diffusion [-] at different matric potentials.

3.11 Air permeability

Similarly to the diffusion data, the air permeability [μm^2] increased from -30 *hPa* to -300 *hPa* (Figures 3.14-3.16). At -30 *hPa*, most samples in the subsoil did not conduct enough air to reach the measurement threshold of 2.3 μm^2 (Figure 3.14b). The air permeability values of the topsoil were highly variable (Figure 3.14a). There were no significant differences between the values of the treatments in the topsoil (p-values: $>$0.24) or in the subsoil (p-values: $>$0.15).

At -100 *hPa*, the air permeability showed high variability in the topsoil (Figure 3.15a). Within the topsoil, there is no significant difference between the values of the treatment (p-values: $>$0.13). In the subsoil, few measurements were above the threshold of 2.3 μm^2 (Figure 3.15b).

At -300 *hPa*, there was still a high variability in the topsoil (Figure 3.16). No significant difference was observed between the values of the treatments in the topsoil (p-values: $>$0.17). In the upper subsoil (30 *cm*), only few values in the *compacted* treatment were above the measurement threshold (Figure 3.16b). The highest air permeability in the upper subsoil was found in the *uncompacted* treatment, which did not differ significantly from the values of the *loosened* treatment (p-value: 0.12). In the lower subsoil (60 *cm*), the air permeability of the *loosened* treatment was strongest but not significantly higher than the values from the *uncompacted* treatment (p-value: 0.08).

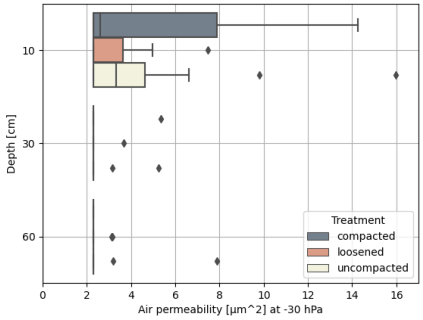

(A) Air permeability [μm^2].

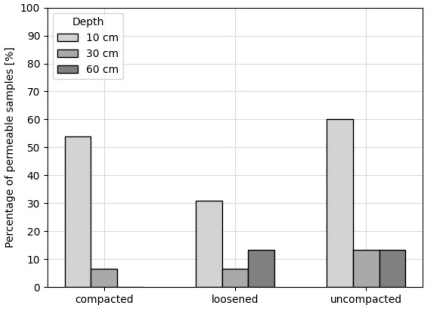

(B) Percentage of permeable samples.

FIGURE 3.14: Air permeability [μm^2] at 30 hPa matric potentials and permeable samples (>2.3 μm^2).

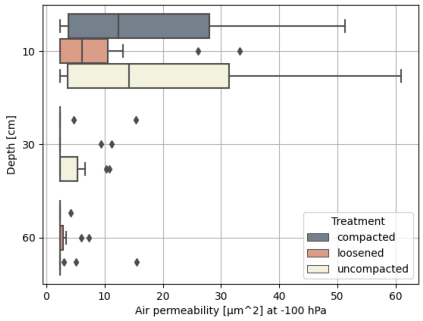

(A) Air permeability [μm^2].

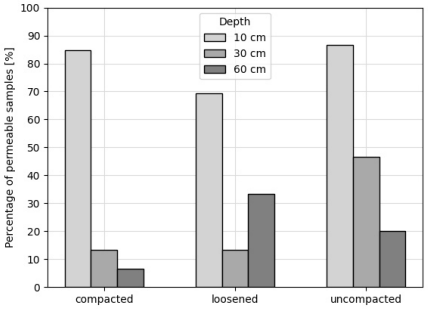

(B) Percentage of permeable samples.

FIGURE 3.15: Air permeability [μm^2] at 100 hPa matric potentials and permeable samples (>2.3 μm^2).

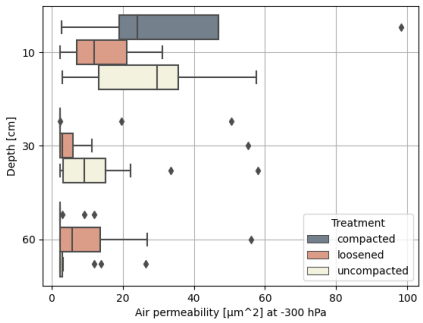

(A) Air permeability [μm^2].

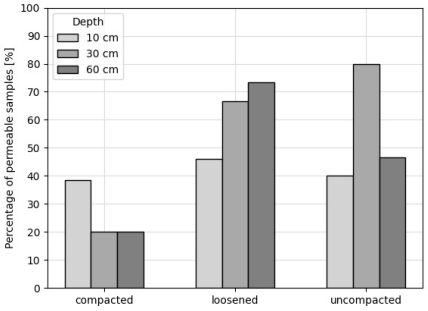

(B) Percentage of permeable samples.

FIGURE 3.16: Air permeability [μm^2] at 300 hPa matric potentials and permeable samples (>2.3 μm^2).

Chapter 4

Discussion

4.1 Alleviation of compaction in the soil matrix

4.1.1 Histogram analysis

Dry bulk density increases naturally with depth (Gao et al., 2016a). The increase from top to subsoil in the gray values in the histograms was more substantial in the *compacted* than in the *uncompacted* treatment. This indicates a rise in soil matrix density, which highlights the compaction in the subsoil (Figure 3.5a and 3.5b).

Mechanical loosening had a remediating effect on soil matrix density since the mode of the *loosened* treatment was significantly lower than the mode of the *compacted* treatment (Figure 3.5b and 3.5c). However, it was not equal to the *uncompacted* treatment, which implies that the soil matrix density is not fully restored. Furthermore, the histogram of the *loosened* treatment showed a higher variability in the soil matrix density. Hence, some parts of the soil matrix were dense, and others were loose. This variability is explained as an outcome of the loosening itself, leaving the soil partially in fragments which are still compacted (Sinnett et al., 2006). Upon visual inspection, compacted fragments were indeed found in the CT images (Figure 3.3b). Apart from fragments, loose and fine particles are also generated by mechanical loosening (Hamza and Anderson, 2005). Additionally, storing the soil samples from October to February may have altered the matrix density and porosity.

4.1.2 Changes in penetration resistance

Soil strength naturally increases with depth due to hydrostatic pressure, internal friction forces, and the weight of the overlying soil material (Richards and Greacen, 1986; Gao et al., 2016a). In the *uncompacted* and *compacted* treatment of November 2021, this behavior was observed (Figure 3.1b). However, in the *compacted* treatment, the rise in penetration resistance was exceptionally high and related to subsoil compaction. Since root growth is restricted above a soil strength of $>2.5\ MPa$, the

subsoil in the *compacted* treatment is almost impenetrable for roots (Gao et al., 2016a).

In chapter 4.1.1, it was shown that mechanical loosening partially lifted compaction. Dry bulk density and penetration resistance are proportional to each other (Gao et al., 2016b). Accordingly, the lowest penetration resistance of the data from November 2021 was expected in the *uncompacted* treatment, where the lowest bulk density occurred. However, the lowest soil strength was observed in the *loosened* treatment. A possible explanation for this unexpected behavior are the fragments created by the loosening (Figure 3.3b). These are quickly displaced upon inserting the penetrometer into the ground and oppose less resistance than an unloosened, uncompacted soil.

Evaluation of the soil strength with penetration resistance measurements is the most commonly used method to assess soil compaction (Fountas et al., 2013). However, this method is highly susceptible to changes in soil moisture and soil texture (Gao et al., 2016b). As seen in Table B.1, the texture did not vary strongly with depth. Hence, soil texture changes were not responsible for the changes in penetration resistance with depth. With low soil water content, the soil gets harder to penetrate (Gao et al., 2016b). The FDR measurements from November 2021 showed approximately even soil moisture with depth (Table B.3). Within the treatments, there was a difference in volumetric water content. However, the soil in the *compacted* treatment was moister than the soil in the *uncompacted* and *loosened* treatment. Therefore, the high penetration resistance of the *compacted* treatment is not due to a lower moisture level but to increased bulk density.

A different measurement device was used to sample in January 2020 (penetrologger), whereas during the measurements in November 2021, a penetrometer was used. During the penetrologger measurements in January 2020, the matric potential of the nearby measurement station differed strongly with depth (Table B.2). Depth-dependent soil moisture contents might have influenced the measurements more strongly in January 2020. Furthermore, the sampling conditions were drier, which explains the generally higher values in January 2020 compared to November 2021. Therefore, the lower penetration resistances in the *compacted* and *uncompacted* treatment of November 2021 were most likely related to moister conditions and a different sampling device and not to natural alleviation of compaction.

Different moisture levels and different measurement device make interannual comparison of the measurements questionable. Therefore, only the difference in penetration resistance between treatments within a year should be analyzed. The penetration resistance of the *compacted* and *loosened* treatment differed strongly in November 2021 (Figure 3.1b). In the measurements before the mechanical loosening in January

2020, the difference in these two plots was not yet significant (Figure 3.1a). Therefore, mechanical loosening efficiently reduced soil strength. Olesen and Munkholm (2007) assessed the effect of subsoil loosening one and a half years after the loosening event and found a similar beneficial effect on penetration resistance. At 30 *cm* depth, penetration resistance was reduced from 2 *MPa* (*compacted*) to 1.5 *MPa* (*loosened*). Their initial compaction level was lower compared to the ROCSUB field. Hence, reduction of penetration resistance by mechanical loosening works for different degrees of initial compaction.

Surprisingly, the penetration resistance of the *uncompacted* plots was relatively high at 2.1±0.4 *MPa* (30 *cm*) and 2.2±0.6 *MPa* (60 *cm*). Etana et al. (2013) measured a similar values for penetration resistance in a compacted subsoil. This suggests that the *uncompacted* treatment of this thesis might have experienced compaction before the experiment started.

4.2 Alteration of macroporosity

The image resolution of the CT images only gives information about macropore diameter of >126 μm. However, in literature, macropore diameters are often defined as >30 μm. Comparing different pore diameters with each other is not advisable. For example, at -30 *hPa* matric potential, pore diameters of 126 μm are drained but pores of 30 μm are not, which may lead to different results in soil aeration measurements. Nevertheless, due to a lack of more suitable data, the values of this thesis (>126 μm pore diameter) were compared to these literature values (>30 μm pore diameter). The soil water retention curve would have offered a better insight into the pore diameters below 126 μm but was unfortunately not ready by the time this thesis was written. Therefore, the following comparisons should be taken with a grain of salt.

The visible macroporosity (>126 μm) in the *compacted* treatment was so low that technical alleviation measures were necessary (Figure 3.6). This arguably improved the macroporosity from 0.2±0.9 vol% to 1.1±2.2 vol% at 60 *cm*. However, Johannes et al. (2021b) suggested a trigger value of 7.7 vol% macroporosity (>30 μm diameter) for subsoils, below which crop production is at risk. Even after loosening the soil mechanically in the ROCSUB field, the macroporosity was still below this trigger value. Johannes et al. (2021b) considered lower macropore diameters (>30 μm), which provides more pore volume than just considering the pore diameters of >126 μm. Hence, the strong difference between the macroporosity of this thesis to the trigger value of Johannes et al. (2021b) might originate from the different pore classes taken into account.

Bochert (1984) studied the outcome of subsoiling in Germany and compared over 60 research sites. According to the author, mechanical subsoil loosening only increased macroporosity (>30 μm diameter) and reduced bulk density if the soil contained >20 % clay and <70 % silt. With a clay-silt ratio <0.3, the subsoil is prone to collapsing instead of loosening (Bochert, 1984; Schneider et al., 2017). Hence, the texture is a significant parameter in compaction remediation. The texture in the ROCSUB field lay within this range of suitable grain size (Table B.1). Therefore, the texture cannot explain the lack of macroporosity improvement by mechanical loosening in this thesis.

Etana et al. (2013) found macroporosity values (>30 μm diameter) of 4.0 vol% (compacted) and 6.4 vol% (control, uncompacted) at 30-35 *cm* depth. At 60 *cm* depth, they measured 7.0 vol% (compacted) and 8.9 vol% (control, uncompacted) at 50-55 *cm* depth. Their values from the *compacted* treatment were closer to the values of this thesis. However, the *uncompacted* treatment of ROCSUB showed a much lower macroporosity than the control of Etana et al. (2013). This underlines again that the *uncompacted* plots at ROCSUB may not be as uncompacted as was assumed at the beginning of the project.

A shift in pore size distribution towards smaller pore diameters with increasing compaction level was observed by Fu et al. (2019), even though the total porosity stopped changing after several traffic passes. Large pores have a weaker internal structure than smaller pores, which makes them more susceptible to compression (Fu et al., 2019). When macropores are crushed, their size is reduced to smaller pore diameters. Therefore, it is essential to consider the pore size distribution and not the total porosity. For example, there was almost no significant change in the visible average pore diameter with depth in the data of this thesis (Figure 3.7). Similarly, the difference in macroporosity (>126 μm) between the treatments was only significant at 60 *cm* depth, where there were nearly no macropores in the *compacted* treatment (Figure 3.6). So, the pore size shift to smaller pores due to compaction was not visible in the macroporosity and average pore diameter.

In the pore size distribution, the picture was drawn more clearly (Figure 3.8). The *uncompacted* treatment showed the most even macropore size distribution, as expected from a subsoil with intact large macropores. Fewer macropores were present in the *compacted* treatment over all diameters since they were crushed under the overlying weight. The *loosened* treatment showed the highest volume of small macropores in the upper subsoil. Mechanical loosening mostly destroys the soil structure and the large macropores (BAFU, 2022; Schneider et al., 2017; Spoor et al., 2003). This results in an abundance of smaller macropores.

4.3 Connectivity of macropores

4.3.1 Percolation

The continuity of macropores is reduced upon compaction (Hemmat and Adamchuk, 2008; Keller et al., 2021; Schäffer et al., 2007). Destruction of connected macropores results in a larger fraction of isolated pore space (Jégou et al., 2002; Schäffer et al., 2007). This was observed in Figure 3.4a, where the *compacted* treatment showed more isolated pores and a lack of connected pores (>126 μm diameter). Similarly, not a single sample of the *compacted* treatment from the lower subsoil showed percolating pores (Figure 3.9b).

A year after loosening the soil mechanically, only 13 % of the *loosened* samples at 30 *cm* depth were percolating, which is exactly the percentage for the *compacted* samples in the upper subsoil (Figure 3.9b). In the *uncompacted* treatment where the soil structure was intact, 67 % of the samples showed a visible connection from top to bottom. A similar picture was drawn in the fraction of percolating pore volume, where only the *uncompacted* treatment showed a percolating porosity of 0.6$\pm$1.2 *vol%* at 30 *cm* depth (Figure 3.9a). Additionally, the only treatment showing a visible median bottleneck diameter was the *uncompacted* treatment (Figure 3.10). Therefore, the *uncompacted* treatment showed a much better connectivity of macropores than in the other treatments.

Considering the percolation threshold (Figure 3.9c), the difference between the *loosened* and *compacted* treatment at 30 *cm* depth is not significant and above their macroporosity. Hence, the macroporosity of both treatments is too low to allow percolation. In the lower subsoil, loosening improved the percolation threshold but still not enough to percolate or match the threshold of the *uncompacted* treatment.

In their review, Schneider et al. (2017) proposed that mechanical loosening could mitigate drought-induced water stress in a compacted soil and make agriculture more resilient to the consequences of climate change. However, the results of this thesis suggest that macropore connectivity and percolation are not necessarily improved with mechanical loosening.

4.3.2 Air diffusion

Diffusivity in soil is the most important gas transport process to ensure respiration of microorganisms and roots (Berisso et al., 2012). In contrast to air permeability, diffusivity does not depend on the minimal pore diameter of a pore network (Keller et al., 2021). Similarly to the air permeability values, the diffusivity showed lower values compared to literature. Keller et al. (2021) measured 0.011 at 30 *cm* and 0.009 at 60 *cm* depth for the *uncompacted* treatment at -100 *hPa*. In this thesis, the values

for the *uncompacted* treatment were 0.004 (30 *cm*) and 0.001 (60 *cm*) at similar matric potential. The *compacted* values of Keller et al. (2021)'s data were 0.005 at 30 and 60 *cm* depth. As already observed in chapter 4.3.3, the *uncompacted* diffusivity values from this thesis were lower than the *compacted* values of Keller et al. (2021). Hence, the *uncompacted* plot might not be as uncompacted as it was assumed when establishing the ROCSUB experiment.

Only at -300 *hPa*, mechanical loosening showed an improvement in diffusivity, where the loosening led to equal values as in the *uncompacted* treatment (Figure 3.13c). However, no significant improvement was found by loosening the soil mechanically at -30 and -100 *hPa*. Zhai and Horn (2019) found an increasing relative diffusivity coefficient after ameliorating the soil mechanically. They measured a value of 0.007 at -300 *hPa*, whereas prior to loosening, the soil exhibited a value of 0.002 under the highest compaction degree. Similar to the ROCSUB values, the loosening had an alleviating effect on diffusion at -300 *hPa*.

4.3.3 Air permeability

According to Fish and Koppi (1994) air permeability measurements are governed by soil structure, particularly by the connectivity and diameter of macropores. The air permeability measured in the laboratory showed low values (Figure 3.14a-3.16a). At field capacity (-100 *hPa*) and higher moisture levels, the subsoil remained almost impermeable to air (Figure 3.15b). Hence, pores with $>$28 μm diameter showed a poor connectivity in all treatments. Only in drier conditions of -300 *hPa*, the subsoil showed air permeability in the *uncompacted* and *loosened* treatment. This suggests that pores drained at this matric potential (9.3 μm diameter) have a better connectivity in the subsoil. However, even at -300 *hPa*, the subsoil remained mostly impermeable in the *compacted* treatment (Figure 3.16b).

The values of air permeability obtained in this thesis were very low in comparison to the values of Keller et al. (2017) that were measured two weeks after compaction. In the *compacted* treatment they measured 4.2 μm^2 (30 *cm* depth) and 3.0 μm^2 (60 *cm* depth). This was close to the values of this thesis ($<$2.3 μm^2). The *uncompacted* treatment at their site showed 17.7 μm^2 (30 *cm* depth) and 10.9 μm^2 (60 *cm* depth) at -100 *hPa*, which was much higher than the $<$2.3 μm^2 measured in the *uncompacted* treatment of this thesis. This indicates that the *uncompacted* plots of this thesis are not well suited as uncompacted reference plots. Since there was no significant difference in air permeability between the *compacted* and *uncompacted* treatment at -100 *hPa* of this thesis, the *uncompacted* treatment was most likely slightly compacted in the past.

Many authors found an increase in air permeability after subsoiling (Drewry and Paton, 2000; Greenwood and Cameron, 1990; Olesen and Munkholm, 2007). Olesen

and Munkholm (2007) found an increase of air permeability due to mechanical loosening from 9.2 μm^2 (compacted) to 14.6 μm^2 (loosened) at 25-29 cm depth and -100 hPa matric potential. The values at the ROCSUB site were much lower and did not increase (both 2.3 μm^2) for the *compacted* and *loosened* treatment. The high variability in the air permeability measurement is explained by the small sample volume (100 cm^3) (Iversen et al., 2001). However, the low air permeability cannot be accounted for by the small cylinder volume, since the studies listed above used the same volumes.

4.3.4 Connectivity and biopores

Biopores offer a high degree of continuity and are very important for air and water transports in soils due to their often vertical orientation (Kautz et al., 2013; Keller et al., 2021; Volkmar, 1996). The ratio of biopores to non-biopores showed a high fraction of biopores in the *uncompacted* treatment (Figure 3.11 and 3.2c). This could explain the better performance of percolation and aeration properties in the *uncompacted* treatment. In Figure 3.4d, the higher connectivity of the pore space in the *uncompacted* sample was clearly visible. Additionally, persistence of biopores increases with soil depth (Dexter, 1991). This is in line with the increasing biopore ratio with depth in the *uncompacted* treatment (Figure 3.11).

In Figure 3.11 both the *compacted* and *loosened* treatment showed a low biopore fraction. Soil compaction disrupts pore networks and negatively affects soil structure (Keller et al., 2021), which explains the low biopore ratio in the *compacted* treatment. As seen in Figure 3.4c, mechanical loosening destroys the inherent soil structure almost completely (BAFU, 2022; Schneider et al., 2017; Spoor et al., 2003). The new formation of biopores takes time since roots need to grow and earthworms to tunnel (BAFU, 2022). Therefore, it was not surprising to observe a low biopore ratio in the *loosened* treatment a year after the mechanical operations. The strong difference in biopore ratio between the *uncompacted* and *loosened* treatment showed that more time is needed for a soil to reform biopores.

4.4 Comparison of methods

Air permeability in the *loosened* treatment seemed to perform equally well as the *uncompacted* treatment (chapter 4.3.3 and 4.3.2). contrary to the behavior the percolating properties (chapter 4.3.1), where the *loosened* treatment showed poorer connectivity than the *uncompacted* treatment. How is it possible to observe such contradicting behavior when percolation and air permeability should both be related to connectivity of macropores? Why was the soil impermeable at -100 hPa but showed percolating properties in the X-ray images?

The percolating properties were calculated by analyzing the X-ray images where the smallest pore diameter visible was 126 μm. However, air permeability and air diffusion were measured in the laboratory. According to equation 2.3, pores of the diameter >28 μm are drained at -100 hPa. Therefore, different pore diameters are compared. In the *loosened* treatment, pores with >126 μm diameter were connected more poorly, whereas pores below 28 μm may be better connected.

The equation of capillary rise is idealized and assumes that the pores are pipes of round shape, which is of course not the case in reality. In soils, pore networks show different shapes and tortuosity. When the soil samples are dried, the large pores drain first but water may occlude smaller pores. This leads to air entrapment, which may influence the air permeability measurements (Luo et al., 2008). The impermeability of the soil samples at -100 hPa could be explained by water remaining in pores and closing off the larger pore behind for gaseous transport (Luo et al., 2008; Stonestrom and Rubin, 1989).

4.5 Inferred consequences for plants and soil biota

So far, the results were discussed on a physical level. However, four important ecosystem services that soils provide are dependent on life in soils (provision of food, nutrient cycling, carbon sequestration, water storage and purification, and habitat for organisms) (FAO and ITPS, 2015). Therefore, in this chapter, the impact of mechanical loosening on plant roots and soil microorganisms is discussed.

Mechanical loosening led to a distinctive decrease in penetration resistance in the subsoil. The soil strength in the *loosened* treatment reached lower values than the *uncompacted* soil and did not exceed the critical soil strength of >2.5 MPa, where most roots cease to grow (Gao et al., 2016a). Hence, mechanical loosening clearly had a beneficial effect on soil strength reduction and is beneficial for root growth. However, by only looking at the root growth from a purely physical perspective, the root's need for sufficient aeration and water is omitted. Most root cells of crops are capable of surviving several hours, e.g. due to water logging, in an oxygen-depleted environment (Drew, 1992). However, under long-term anoxic conditions, most roots will die.

Fish and Koppi (1994) found a limiting threshold of air permeability of 20 μm^2 for root growth in soils. In the subsoil of the ROCSUB site, this threshold was not exceeded for -30 and -100 hPa by any treatment. At -300 hPa, only single measurements were above 20 μm^2, which implies that this subsoil is generally poorly aerated in every treatment (Berisso et al., 2012). The relative diffusivity confirms these findings.

A satisfactory relative diffusivity coefficient of 0.005-0.02 for root growth was determined by Stepniewski (1980). For aerobic microbial activity, the threshold lies at 0.005 (Berisso et al., 2012; Schjønning et al., 2003). The threshold of 0.005 was rarely reached at field capacity (-100 hPa) and almost never at -30 hPa. Only at -300 hPa, the *loosened* and *uncompacted* treatment managed to provide sufficiently high diffusion values to sustain aerobic microbial activity and root growth in the subsoil. Hence, the subsoil of the ROCSUB field experiences regularly oxygen-depleted conditions and might even exhibit anoxic regions under high levels of moisture, especially in the *compacted* plots.

In light of the suitability of the soil for plant growth, the POM content should not be forgotten. The *compacted* treatment exhibits poor conditions for root growth with its high soil strength, low aeration, poor connectivity for percolation, and small macroporosity. Unsurprisingly, this led to very low POM contents in the subsoil of the *compacted* treatment (Figure 3.12).
The *loosened* treatment showed an equal POM content as in the *uncompacted* treatment in the subsoil. In the *loosened* treatment, the roots benefited from the low penetration resistance, whereas in the *uncompacted* treatment, the macropores were better connected and more biopores were present. According to literature, higher biopore abundance is beneficial for root growth, since roots preferentially reuse biopores, where they grow faster (Kautz et al., 2013; Wahlström et al., 2021). Another explanation for the almost even POM content in the *loosened* and *uncompacted* treatment is presented in the air permeability and air diffusion (Figure 3.13a-3.16b). Colombi et al. (2019) linked higher organic carbon content to improved gas transportation ability in tilled subsoils, which resulted in better growing conditions for roots. At low moisture levels, the *loosened* and *uncompacted* treatment shared similar air permeability and air diffusion.

However, POM content might not be the best predictor for root growth conditions. Under low oxygen supply, decomposition of organic material is limited (Parr and Reuszer, 1962). Hence, high POM content could also be linked to poor degradation ability. This occurs, when the ROCSUB soil reaches field capacity and air permeability and air diffusion is lowered.

Chapter 5

Conclusion

The goal of this master thesis was to assess the effect of mechanical loosening a year later on different physical soil properties and structure in a severely compacted subsoil. The following research question and hypotheses were stated in the beginning of this thesis:

1. How does mechanical loosening of a heavily compacted subsoil affect soil physical properties and structure?
2. **Hypothesis 1**: Loosening as an ameliorative mechanical operation yields significant improvements regarding physical soil structure and properties compared to compacted soil.
3. **Hypothesis 2**: Within one year, soil structure and properties are not restored completely compared to an uncompacted soil

Mechanical loosening significantly improved many soil properties compared to severely compacted soil. Penetration resistance was strongly reduced, soil matrix density was lowered, and macroporosity increased at 60 *cm* depth. Additionally, the pore size distribution of the *loosened* treatment showed more pores over all diameters in comparison to the *compacted* treatment. Loosening led to an increase in POM content.

Loosening only improved air diffusion and air permeability at -300 *hPa*, where smaller pores were drained. However, almost no improvements by mechanical loosening were found in the percolating properties. The median bottleneck diameter did not improve significantly and neither did the biopore ratio in the subsoil. Hence, properties linked to connectivity only showed an improvement owing to mechanical loosening at the mesopore scale ($<$28 μm pore diameter). Even though connectivity was not improved throughout all pore diameters, most physical properties showed strong improvements after mechanical loosening. Therefore, the first hypothesis was accepted.

One year after loosening the *compacted* soil, there were still significant differences between the *loosened* and the *uncompacted* treatment. The soil matrix density of the *loosened* treatment was significantly different from the *uncompacted* treatment. The pore

size distribution of the *loosened* treatment showed an uneven distribution compared to the *uncompacted* treatment. However, the macroporosity was similar and the penetration resistance was lower in the *loosened* treatment. The *uncompacted* treatment showed higher connectivity and biopore ratio than the *loosened* treatment one year after loosening. However, at smaller pore diameters ($<28\ \mu m$), the *loosened* soil performed equally well regarding soil aeration. Since most physical soil properties still differed between the *loosened* and *uncompacted* treatment and connectivity was not yet fully restored, the second hypothesis was accepted.

It will be interesting to observe the development of the ROCSUB field over the years. With the increase of biopores over time, the connectivity in the *loosened* treatment will hopefully improve. As a result, water infiltration and aeration are bound to increase. Due to time constrains, it was not possible to include the soil water retention curve, which would have shed light on the meso- and micropore distribution. Additionally, studying the *loosened* treatment's resistance to withstand mechanical stress would make an interesting topic for future research since loosened soils are prone to recompaction.

Under vulnerable circumstances, the time it takes for a soil to get compacted lies below a minute. Driving over the field with high axial load at the wrong time is all it takes for a soil to strongly reduce its ecosystem functions over several years. The recovery process is slow and can be supported by mechanical loosening. As seen in this thesis, mechanical operations improve many physical properties in soils. However, the vital connectivity of macropores for fluid transportation in soils is not necessarily restored. Within a year, the formation of biopores did not progress enough to ensure macropore connectivity in the loosened soil. Hence, mechanical loosening cannot instantaneously restore a soil. Since civilization strongly depends on intact soils, the focus should lie on treating the soils more sustainably and emphasizing the prevention of compaction.

Appendix A

Data tables

The accuracy of the measurement device defines the amount of decimal places. The air diffusion is usually given with three decimal places after the comma, according to literature.

TABLE A.1: Median of penetration resistance [MPa] measured on January 2020 by Alice Johannes with a penetrologger and measured on November 2021 by Alina Widmer with a penetrometer.

Treatment	**Depth** [cm]	**Penetration resistance** [MPa]	**Penetration resistance** [MPa]
Date		Jan 20	Nov 21
compacted	10	2.4±0.8	1.2±0.6
loosened	10	2.5±0.4	1.1±0.3
uncompacted	10	2.6±0.4	1.1±0.4
compacted	30	4.6±1.2	3.2±1.1
loosened	30	3.8±0.6	1.3±0.6
uncompacted	30	3.0±0.5	2.1±0.4
compacted	60	5.3±0.4	3.6±0.9
loosened	60	4.5±0.6	1.7±1.0
uncompacted	60	3.1±0.4	2.2±0.6

TABLE A.2: Median macroporosity [*vol%*] and median pore diameter [*mm*] derived from CT images (for pore diameters >126 μm).

Treatment	**Depth** [*cm*]	**Macroporosity** [*vol%*]	**Average pore diameter** [*mm*]
compacted	10	8.6±4.2	0.2±0.0
loosened	10	5.2±2.1	0.2±0.1
uncompacted	10	8.1±3.1	0.3±0.1
compacted	30	1.1±2.0	0.2±0.2
loosened	30	2.1±1.8	0.2±0.1
uncompacted	30	2.5±1.2	0.2±0.1
compacted	60	0.2±0.9	0.2±0.3
loosened	60	1.1±2.2	0.2±0.1
uncompacted	60	1.0±1.0	0.2±0.1

TABLE A.3: Median percolating volume fraction [*vol%*] and median percolation threshold [*vol%*] derived from CT images (for pore diameters >126 μm).

Treatment	**Depth** [*cm*]	**Percolating volume fraction** [*vol%*]	**Percolation threshold** [*vol%*]
compacted	10	7.6±5.2	5.5±5.4
loosened	10	0.0±2.3	8.2±5.0
uncompacted	10	5.9±3.8	2.9±4.1
compacted	30	0.0±1.5	10.6±17.7
loosened	30	0.0±1.4	12.1±8.5
uncompacted	30	0.6±1.2	1.4±3.9
compacted	60	0.0±0.0	24.4±7.9
loosened	60	0.0±0.0	13.6±10.6
uncompacted	60	0.0±0.6	1.6±6.6

TABLE A.4: Median bottleneck diameter, median biopore ratio, and median POM content [*vol%*] derived from CT images (for pore diameters >126 μm).

Treatment	**Depth** [*cm*]	**Bottleneck diameter** [*mm*]	**Biopore ratio** [-]	**POM content** [*vol%*]
compacted	10	0.2±0.2	1.2±0.5	6.4±3.0
loosened	10	0.0±0.2	1.0±0.3	5.9±1.5
uncompacted	10	0.4±0.4	1.5±0.7	3.0±0.8
compacted	30	0.0±0.2	0.8±0.4	0.6±0.9
loosened	30	0.0±0.1	1.3±0.4	1.4±0.6
uncompacted	30	0.2±0.5	1.8±0.8	1.4±0.4
compacted	60	0.0±0.0	1.7±1.1	0.1±0.1
loosened	60	0.0±0.1	1.1±0.5	0.4±0.7
uncompacted	60	0.0±0.2	2.7±1.1	0.8±0.4

TABLE A.5: Median of air permeability [μm^2] measurements at different matric potentials by Marlies Sommer.

Treatment	**Depth** [cm]	**-30** hPa	**-100** hPa	**-300** hPa
compacted	10	2.6±4.0	12.4±16.2	24.1±33.2
loosened	10	2.3±1.8	4.3±8.7	7.2±10.3
uncompacted	10	3.3±3.7	14.2±19.1	29.6±18.1
compacted	30	2.3±0.8	2.3±3.3	2.3±12.9
loosened	30	2.3±0.3	2.3±2.7	3.1±13.8
uncompacted	30	2.3±0.7	2.3±2.8	9.3±15.0
compacted	60	2.3±0.0	2.3±0.5	2.3±2.8
loosened	60	2.3±0.3	2.3±1.5	5.8±14.3
uncompacted	60	2.3±1.4	2.3±3.3	2.3±6.7

TABLE A.6: Median of relative gas diffusivity coefficient $\left[\frac{D_p}{D_o}\right]$ [-] measurements at different matric potentials by Marlies Sommer.

Treatment	**Depth** [cm]	**-30** hPa	**-100** hPa	**-300** hPa
compacted	10	0.001±0.003	0.009±0.008	0.020±0.012
loosened	10	0.002±0.002	0.007±0.005	0.007±0.008
uncompacted	10	0.002±0.002	0.010±0.008	0.017±0.004
compacted	30	0.001±0.002	0.001±0.004	0.005±0.007
loosened	30	0.001±0.001	0.001±0.003	0.011±0.006
uncompacted	30	0.001±0.001	0.004±0.003	0.010±0.005
compacted	60	0.001±0.001	0.001±0.002	0.004±0.003
loosened	60	0.000±0.001	0.001±0.002	0.009±0.007
uncompacted	60	0.001±0.001	0.001±0.002	0.006±0.003

Appendix B

Supplementary tables

TABLE B.1: Soil texture of ROCSUB field with each fraction in % provided by Alice Johannes.

Depth	**Clay** [%]	**Silt** [%]	**Sand** [%]
0-20 *cm*	26.3 ± 2.0	43.0 ± 0.9	30.8 ± 2.3
10-20 *cm*	26.2 ± 2.0	43.7 ± 0.9	30.1 ± 2.3
20-50 *cm*	27.5 ± 2.9	44.1 ± 1.6	28.4 ± 3.1
total	26.7 ± 2.4	43.6 ± 1.3	29.8 ± 2.5

TABLE B.2: Matric potential Ψ measurements at Changins measured with a tensiometer (Meteotest, 2022).

Depth $[cm]$	**22.01.2020** Ψ $[hPa]$	**04.11.2022** Ψ $[hPa]$
10-20	-34	-17
30-35	-25	-13
60	-51	-10

TABLE B.3: Mean of the volumetric water content θ measurements done with a frequency domain reflectometry (FDR) on 04.11.2021.

Depth $[cm]$	**Compacted** $\theta \left[\frac{m^3}{m^3}\right]$	**Loosened** $\theta \left[\frac{m^3}{m^3}\right]$	**Uncompacted** $\theta \left[\frac{m^3}{m^3}\right]$	**Mean** $\theta \left[\frac{m^3}{m^3}\right]$
15	0.34	0.32	0.31	0.33
35	0.35	0.33	0.33	0.34
60	0.37	0.37	0.32	0.35

Appendix C

Macros and programs

C.1 Macro: Conversion from raw to tiff format

```
dir_import = getDirectory("E:\RocSub\20220217_ROCSUB");
list = getFileList(dir_import); // liste von scanbilder-ordnern
dir_save = getDirectory("C:\Users\X60028558\Documents\XRay_img_all_tiff");

for (i=0; i<list.length; i++){
    list_corr = list[i];
    dir_all = dir_import + list_corr; //Directory zu Unterordner, wo .vol-Datei drin
    dir_all = dir_all.replace("\\", "/"); // Backslashs und / sind vertauscht -> ersetzen
    name_allfiles = getFileList(dir_all); // Liste mit allen Dateien in diesem Unterordner (inkl. .Vol-Datei)
    for (j = 0; j < name_allfiles.length; j++){
        if (endsWith(name_allfiles[j], ".vol"))
            name_vol = name_allfiles[j];
            }
    dir_vol = dir_import + list_corr + name_vol ; // Directory zusammenfrankensteinen
    dir_vol = dir_vol.replace("\\", "/"); // Backslashs und / sind vertauscht -> ersetzen
    run("Raw...", "open=" + dir_vol + " image=[16-bit Unsigned] width=1012 height=1012 number=1012 little-endian");
    name_vol = name_vol.substring(0, name_vol.length() -4); //.vol-Endung wegschnipseln
    saveAs("Tiff", dir_save + name_vol + ".tif");
    close();
}
```

C.2 Macro: Adaptive Gaussian filtering

```
dir_in = getDirectory("E:\RocSub\20220217_ROCSUB");
allfiles = getFileList(dir_in);
dir_out = getDirectory("C:\Users\X60028558\Documents\XRay_img_all_tiff");


for (i = 1; i < allfiles.length; i++){
    print(allfiles[i]);
    if (endsWith(allfiles[i], "tif")){
        open(dir_in + allfiles[i]);
        run("Enhance Contrast", "saturated=0.35");
        run("3D Fast Filters","filter=Adaptive radius_x_pix=2.0 radius_y_pix=2.0 radius_z_pix=2.0 Nb_cpus=8");
        selectWindow(allfiles[i]);
        close();
        selectWindow("3D_Adaptive");
        run("Macro...", "code=[if(v==0) v = 1] stack");
        saveAs("Tiff", dir_out + allfiles[i]);
        close();
    }
}
```

C.3 Gray scale calibration

```
import numpy as np
import os
import glob
import pandas as pd
import tifffile as tif
import cv2

os.chdir(r"E:\RocSub\TIFF\StraightAndCentered\WallCoordinateIdentified\Adap
tiveGaussian")
filenames = [i for i in glob.glob("*.tif")]


luft = pd.read_csv("Kalibrationswerte.csv", delimiter=";")
luft_name = luft.iloc[:,0].tolist()
luft_value = luft.iloc[:,1].tolist()
alu_value = luft.iloc[:,2].tolist()

uTarget = 20000.0
lTarget = 5000.0


for i in range(len(filenames)):

os.chdir(r"E:\RocSub\TIFF\StraightAndCentered\WallCoordinateIdentified\Adap
tiveGaussian")
    im = cv2.imreadmulti(filenames[i], flags = cv2.IMREAD_UNCHANGED)
    im = im[1]
    im = np.array(im)
    for j in range(len(luft_name)):
        if luft_name[j] == filenames[i]:
            lower = float(luft_value[j])
            upper = float(alu_value[j])
            print(lower)
    easy_way = (im.astype(float) - lower) * ((uTarget - lTarget) / (upper -
lower)) + lTarget  # ohne Float funktioniert Rechnung nicht!
    easy_way = easy_way.astype(int)
    easy_way = easy_way.clip(0, 65535)
    easy_way = easy_way.astype("uint16") #unbedingt unsigned, sonst gibt es
bei den höchsten Werten (über 2^15 = 32k) negative Werte draus, weil ein
Bit (signed) für VZ verwendet wird

os.chdir(r"E:\RocSub\TIFF\StraightAndCentered\WallCoordinateIdentified\Adap
tiveGaussian\Calibrated")
    tif.imwrite(filenames[i], easy_way)
```

Bibliography

Agroscope (2018). "Air permeability". Zürich, Reckenholz, pp. 1-2.

Agroscope (2019). "Gas diffusivity". Zürich, Reckenholz, pp. 1-3.

BAFU (2022). "Sachgerechter Umgang mit Boden beim Bauen Sachgerechter Umgang mit Boden beim Bauen. Ein Modul der Vollzugshilfe Bodenschutz beim Bauen". Bundesamt für Umwelt, Bodenschutz, Bern, pp. 1-34.

Batey, T. (2009). "Soil compaction and soil management - a review". In: *Soil Use and Management* 25.4, pp. 335–345. ISSN: 02660032. DOI: 10.1111/j.1475-2743.2009.00236.x. URL: https://onlinelibrary.wiley.com/doi/10.1111/j.1475-2743.2009.00236.x.

Batey, T. and D. C. McKenzie (2006). "Soil compaction: identification directly in the field". In: *Soil Use and Management* 22.2, pp. 123–131. ISSN: 0266-0032. DOI: 10.1111/j.1475-2743.2006.00017.x. URL: https://onlinelibrary.wiley.com/doi/10.1111/j.1475-2743.2006.00017.x.

Berisso, F. E., P. Schjønning, T. Keller, M. Lamandé, A. Etana, L. W. De Jonge, B. V. Iversen, J. Arvidsson, and J. Forkman (2012). "Persistent effects of subsoil compaction on pore size distribution and gas transport in a loamy soil". In: *Soil and Tillage Research* 122, pp. 42–51. ISSN: 01671987. DOI: 10.1016/j.still.2012.02.005.

Bochert, H. (1984). "Grenzen und Vorhersage der Bodenmeliorationswirkung bei der Tieflockerung". In: *Mitteilungen der Deutschen Bodenkundlichen Gesellschaft* 40, pp. 37–40.

Bonnard, L.F. (1982). "Carte des sols du domaine de Changins (VD)". Zürich, Reckenholz. [last accessed: 24.08.2022]. URL: https://www.nabodat.ch/images/design/karten/boka_gm/FAP_128_0185.1.jpg.

Brus, D. J. and J. J. H. van den Akker (2018). "How serious a problem is subsoil compaction in the Netherlands? A survey based on probability sampling". In: *SOIL* 4.1, pp. 37–45. ISSN: 2199-398X. DOI: 10.5194/soil-4-37-2018. URL: https://soil.copernicus.org/articles/4/37/2018/.

Chen, G. and R. R. Weil (2010). "Penetration of cover crop roots through compacted soils". In: *Plant and Soil* 331.1-2, pp. 31–43. ISSN: 0032-079X. DOI: 10.1007/s11104-009-0223-7. URL: http://link.springer.com/10.1007/s11104-009-0223-7.

Colombi, T., F. Walder, L. Büchi, M. Sommer, K. Liu, J. Six, M. G. A. van der Heijden, R. Charles, and T. Keller (2019). "On-farm study reveals positive relationship between gas transport capacity and organic carbon content in arable soil". In:

SOIL 5.1, pp. 91–105. ISSN: 2199-398X. DOI: 10.5194/soil-5-91-2019. URL: https://soil.copernicus.org/articles/5/91/2019/.

Cresswell, H. P. and J. A. Kirkegaard (1995). "Subsoil amelioration by plant-roots - the process and the evidence". In: *Soil Research* 33.2, pp. 221–239. ISSN: 1838-675X. DOI: 10.1071/SR9950221. URL: http://www.publish.csiro.au/?paper=SR9950221.

DeJong-Hughes, J. (2018). "Soil compaction". In: *Crop Production*. Ed. by University of Minnesota Extension. [last accessed: 24.08.2022]. URL: https://extension.umn.edu/soil-management-and-health/soil-compaction.

Dexter, A.R. (1991). "Amelioration of soil by natural processes". In: *Soil and Tillage Research* 20.1, pp. 87–100. ISSN: 01671987. DOI: 10.1016/0167-1987(91)90127-J. URL: https://linkinghub.elsevier.com/retrieve/pii/016719879190127J.

Doube, M., M. M. Kłosowski, I. Arganda-Carreras, F. P. Cordelières, R. P. Dougherty, J. S. Jackson, B. Schmid, J. R. Hutchinson, and S. J. Shefelbine (2010). "BoneJ: Free and extensible bone image analysis in ImageJ". In: *Bone* 47.6, pp. 1076–1079. ISSN: 87563282. DOI: 10.1016/j.bone.2010.08.023. URL: https://linkinghub.elsevier.com/retrieve/pii/S8756328210014419.

Drew, M. C. (1992). "Soil aeration and plant root metabolism". In: *Soil Science* 154.4, pp. 259–268.

Drewry, J. J. and R. J. Paton (2000). "Effect of subsoiling on soil physical properties and dry matter production on a Brown Soil in Southland, New Zealand". In: *New Zealand Journal of Agricultural Research* 43.2, pp. 259–268. ISSN: 00288233. DOI: 10.1080/00288233.2000.9513426.

Eijkelkamp (2018a). "Hand penetrometer Eijkelkamp - 1 m or 3 m 06.01". [last accessed: 24.08.2022]. URL: https://www.royaleijkelkamp.com/products/field-measuring-equipment/resistance-to-penetration/mechanical/hand-penetrometer-eijkelkamp-1-m-or-3-m/.

Eijkelkamp (2018b). "Penetrologger with GPS - standard set 06.15.SA". [last accessed: 24.08.2022]. URL: https://www.royaleijkelkamp.com/products/field-measuring-equipment/resistance-to-penetration/electronic-with-datalogger/penetrologger-with-gps-standard-set/.

Eijkelkamp (2019). "Soil sampling ring kit - model C53". [last accessed: 24.08.2022]. URL: https://www.royaleijkelkamp.com/products/augers-samplers/soil-augers-samplers/undisturbed-core-samplers/soil-sampling-ring-kit-model-c53/.

Etana, A., M. Larsbo, T. Keller, J. Arvidsson, P. Schjønning, J. Forkman, and N. Jarvis (2013). "Persistent subsoil compaction and its effects on preferential flow patterns in a loamy till soil". In: *Geoderma* 192.1, pp. 430–436. ISSN: 00167061. DOI: 10.1016/j.geoderma.2012.08.015. URL: http://dx.doi.org/10.1016/j.geoderma.2012.08.015.

FAO and ITPS (2015). "Status of the World's Soil Resources (SWSR) - Main Report". Rome, Italy. [last accessed: 24.08.2022]. URL: https://www.fao.org/3/bc590e/bc590e.pdf.

Fish, A.N. and A.J. Koppi (1994). "The use of a simple field air permeameter as a rapid indicator of functional soil pore space". In: *Geoderma* 63.3-4, pp. 255–264. ISSN: 00167061. DOI: 10.1016/0016-7061(94)90067-1. URL: https://linkinghub.elsevier.com/retrieve/pii/0016706194900671.

Fountas, S., D. Paraforos, C. Cavalaris, C. Karamoutis, T. A. Gemtos, N. Abu-Khalaf, and A. Tagarakis (2013). "A five-point penetrometer with GPS for measuring soil compaction variability". In: *Computers and Electronics in Agriculture* 96, pp. 109–116. ISSN: 01681699. DOI: 10.1016/j.compag.2013.04.018. URL: https://linkinghub.elsevier.com/retrieve/pii/S016816991300104X.

Fu, Y., Z. Tian, A. Amoozegar, and J. Heitman (2019). "Measuring dynamic changes of soil porosity during compaction". In: *Soil and Tillage Research* 193.1, pp. 114–121. ISSN: 01671987. DOI: 10.1016/j.still.2019.05.016. URL: https://doi.org/10.1016/j.still.2019.05.016.

Gao, W., L. Hodgkinson, K. Jin, C.W. Watts, R.W. Ashton, J. Shen, T. Ren, I.C. Dodd, A. Binley, A.L. Phillips, P. Hedden, M. J. Hawkesford, and W.R. Whalley (2016a). "Deep roots and soil structure". In: *Plant, Cell & Environment* 39.8, pp. 1662–1668. ISSN: 01407791. DOI: 10.1111/pce.12684. URL: https://onlinelibrary.wiley.com/doi/10.1111/pce.12684.

Gao, W., W. R. Whalley, Z. Tian, J. Liu, and T. Ren (2016b). "A simple model to predict soil penetrometer resistance as a function of density, drying and depth in the field". In: *Soil and Tillage Research* 155, pp. 190–198. ISSN: 01671987. DOI: 10.1016/j.still.2015.08.004. URL: https://linkinghub.elsevier.com/retrieve/pii/S0167198715300027.

Greenwood, P.B. and K.C. Cameron (1990). "Subsoiling research in North Otago and Canterbury: an overview". In: *Proceedings of the 5th national Land Drainage Conference.* Massey University, pp. 38–59.

Håkansson, I. and R. C. Reeder (1994). "Subsoil compaction by vehicles with high axle load—extent, persistence and crop response". In: *Soil and Tillage Research* 29.2-3, pp. 277–304. ISSN: 01671987. DOI: 10.1016/0167-1987(94)90065-5. URL: https://linkinghub.elsevier.com/retrieve/pii/0167198794900655.

Hammel, J.E. (1994). "Effect of high-axle load traffic on subsoil physical properties and crop yields in the Pacific Northwest USA". In: *Soil and Tillage Research* 29.2-3, pp. 195–203. ISSN: 01671987. DOI: 10.1016/0167-1987(94)90057-4. URL: https://linkinghub.elsevier.com/retrieve/pii/0167198794900574.

Hamza, M. A. and W. K. Anderson (2005). "Soil compaction in cropping systems: A review of the nature, causes and possible solutions". In: *Soil and Tillage Research* 82.2, pp. 121–145. ISSN: 01671987. DOI: 10.1016/j.still.2004.08.009.

Hemmat, A. and V. I. Adamchuk (2008). "Sensor systems for measuring soil compaction: Review and analysis". In: *Computers and Electronics in Agriculture* 63.2, pp. 89–103. ISSN: 01681699. DOI: 10.1016/j.compag.2008.03.001.

Hendriks, M. R. (2010). "Soil water". In: *Introduction to physical Hydrology*. Oxford: Oxford University Press, pp. 141–196. ISBN: 9780199296842.

IPCC (2022). "Summary for Policymakers". In: *Climate Change 2022: Impacts, Adaptation and Vulnerability*. Ed. by E.S. Poloczanska K. Mintenbeck M. Tignor H.-O. Pörtner D.C. Roberts and S. Langsdorf S. Löschke V. Möller A. Okem A. Alegría M. Craig. Cambridge & New York: Cambridge University Press. Chap. Contributi, pp. 3–33. DOI: 10.1017/9781009325844.001.

Iversen, B. V., P. Schjønning, T. G. Poulsen, and P. Moldrup (2001). "In situ, on-site and laboratory measurements of soil air permeability: Boundary conditions and measurement scale". In: *Soil Science* 166.2, pp. 97–106. ISSN: 0038075X. DOI: 10.1097/00010694-200102000-00003.

Jarvis, N. J. (2007). "A review of non-equilibrium water flow and solute transport in soil macropores: principles, controlling factors and consequences for water quality". In: *European Journal of Soil Science* 58.3, pp. 523–546. ISSN: 1351-0754. DOI: 10.1111/j.1365-2389.2007.00915.x. URL: https://onlinelibrary.wiley.com/doi/10.1111/j.1365-2389.2007.00915.x.

Jégou, D., J. Brunotte, H. Rogasik, Y. Capowiez, H. Diestel, S. Schrader, and D. Cluzeau (2002). "Impact of soil compaction on earthworm burrow systems using X-ray computed tomography: preliminary study". In: *European Journal of Soil Biology* 38.3-4, pp. 329–336. ISSN: 11645563. DOI: 10.1016/S1164-5563(02)01148-2. URL: https://linkinghub.elsevier.com/retrieve/pii/S1164556302011482.

Johannes, A., S. Sinaj, L. Bragazza, J. Koestel, T. Keller, and P. Weisskopf (2021a). "Wiederherstellung eines schadverdichteten Unterbodens". Agroscope, Zürich & Nyon, pp. 1-18.

Johannes, A., P. Weisskopf, and P. Boivin (2021b). "Soil structure degradation evaluation for environmental legislation (STRUDEL)". Agroscope, Zürich, Reckenholz, pp. 1-62.

Kautz, T., W. Amelung, F. Ewert, T. Gaiser, R. Horn, R. Jahn, M. Javaux, A. Kemna, Y. Kuzyakov, J. Munch, S. Pätzold, S. Peth, H. W. Scherer, M. Schloter, H. Schneider, J. Vanderborght, D. Vetterlein, A. Walter, G. L.B. Wiesenberg, and U. Köpke (2013). "Nutrient acquisition from arable subsoils in temperate climates: A review". In: *Soil Biology and Biochemistry* 57, pp. 1003–1022. ISSN: 00380717. DOI: 10.1016/j.soilbio.2012.09.014. URL: http://dx.doi.org/10.1016/j.soilbio.2012.09.014.

Keller, T., T. Colombi, S. Ruiz, M. P. Manalili, J. Rek, V. Stadelmann, H. Wunderli, D. Breitenstein, R. Reiser, H. Oberholzer, S. Schymanski, A. Romero-Ruiz, N. Linde, P. Weisskopf, A. Walter, and D. Or (2017). "Long-Term Soil Structure Observatory for Monitoring Post-Compaction Evolution of Soil Structure". In: *Vadose Zone Journal* 16.4, pp. 1–16. ISSN: 1539-1663. DOI: 10.2136/vzj2016.11.0118.

Keller, T., T. Colombi, S. Ruiz, S. J. Schymanski, P. Weisskopf, J. Koestel, M. Sommer, V. Stadelmann, D. Breitenstein, N. Kirchgessner, A. Walter, and D. Or (2021). "Soil structure recovery following compaction: Short-term evolution of soil physical properties in a loamy soil". In: *Soil Science Society of America Journal* 85.4, pp. 1002–1020. ISSN: 14350661. DOI: 10.1002/saj2.20240.

Keller, T. and D. Or (2022). "Farm vehicles approaching weights of sauropods exceed safe mechanical limits for soil functioning". In: *Proceedings of the National Academy of Sciences* 119.21, pp. 1–6. ISSN: 0027-8424. DOI: 10.1073/pnas.2117699119. URL: https://pnas.org/doi/full/10.1073/pnas.2117699119.

Keller, T., M. Sandin, T. Colombi, R. Horn, and D. Or (2019). "Historical increase in agricultural machinery weights enhanced soil stress levels and adversely affected soil functioning". In: *Soil and Tillage Research* 194.1, pp. 1–12. ISSN: 01671987. DOI: 10.1016/j.still.2019.104293. URL: https://doi.org/10.1016/j.still.2019.104293.

Koestel, J. (2018). "SoilJ: An ImageJ Plugin for the Semiautomatic Processing of Three-Dimensional X-ray Images of Soils". In: *Vadose Zone Journal* 17.1, pp. 1–7. ISSN: 15391663. DOI: 10.2136/vzj2017.03.0062. URL: http://doi.wiley.com/10.2136/vzj2017.03.0062.

Lamandé, M., D. Wildenschild, F. E. Berisso, A. Garbout, M. Marsh, P. Moldrup, T. Keller, S. B. Hansen, L. W. De Jonge, and P. Schjønning (2013). "X-ray CT and laboratory measurements on glacial till subsoil cores: Assessment of inherent and compaction-affected soil structure characteristics". In: *Soil Science* 178.7, pp. 359–368. ISSN: 0038075X. DOI: 10.1097/SS.0b013e3182a79e1a.

Lipiec, J. and R. Hatano (2003). "Quantification of compaction effects on soil physical properties and crop growth". In: *Geoderma* 116.1-2, pp. 107–136. ISSN: 00167061. DOI: 10.1016/S0016-7061(03)00097-1. URL: https://linkinghub.elsevier.com/retrieve/pii/S0016706103000971.

Luo, L., H. Lin, and P. Halleck (2008). "Quantifying Soil Structure and Preferential Flow in Intact Soil Using X-ray Computed Tomography". In: *Soil Science Society of America Journal* 72.4, pp. 1058–1069. ISSN: 03615995. DOI: 10.2136/sssaj2007.0179. URL: http://doi.wiley.com/10.2136/sssaj2007.0179.

Meteotest (2022). "Bodenmessnetz Nordwestschweiz". Standort Changins, [last accessed: 24.08.2022]. URL: https://bodenmessnetz.ch/messwerte/aktuelle_daten/changins.

Munkholm, L. J., P. Schjønning, M. H. Jørgensen, and K. Thorup-Kristensen (2005). "Mitigation of subsoil recompaction by light traffic and on-land ploughing". In: *Soil and Tillage Research* 80.1-2, pp. 159–170. ISSN: 01671987. DOI: 10.1016/j.still.2004.03.016. URL: https://linkinghub.elsevier.com/retrieve/pii/S016719870400100X.

Olesen, J. and L. Munkholm (2007). "Subsoil loosening in a crop rotation for organic farming eliminated plough pan with mixed effects on crop yield". In: *Soil and Tillage Research* 94.2, pp. 376–385. ISSN: 01671987. DOI: 10.1016/j.still.

2006.08.015. URL: https://linkinghub.elsevier.com/retrieve/pii/S0167198706002005.

Ollion, J., J. Cochennec, F. Loll, C. Escudé, and T. Boudier (2013). "TANGO: a generic tool for high-throughput 3D image analysis for studying nuclear organization". In: *Bioinformatics* 29.14, pp. 1840–1841. ISSN: 1460-2059. DOI: 10.1093/bioinformatics/btt276. URL: https://academic.oup.com/bioinformatics/article-lookup/doi/10.1093/bioinformatics/btt276.

Parr, J. F. and H. W. Reuszer (1962). "Organic Matter Decomposition as Influenced by Oxygen Level and Flow Rate of Gases in the Constant Aeration Method". In: *Soil Science Society of America Journal* 26.6, pp. 552–556. ISSN: 03615995. DOI: 10.2136/sssaj1962.03615995002600060012x. URL: http://doi.wiley.com/10.2136/sssaj1962.03615995002600060012x.

Richards, B. G. and E. L. Greacen (1986). "Mechanical stresses on an expanding cylindrical root analog in antigranulocytes media". In: *Soil Research* 24.3, pp. 393–404. ISSN: 1838-675X. DOI: 10.1071/SR9860393. URL: http://www.publish.csiro.au/?paper=SR9860393.

Rumpel, C. and I. Kögel-Knabner (2011). "Deep soil organic matter—a key but poorly understood component of terrestrial C cycle". In: *Plant and Soil* 338.1-2, pp. 143–158. ISSN: 0032-079X. DOI: 10.1007/s11104-010-0391-5. URL: http://link.springer.com/10.1007/s11104-010-0391-5.

Salvador, N., S.H. Benez, and R. L. Mion (2009). "Energy demand in the subsoiling performed before and after different systems of periodic soil tillage/ Demanda energetica na subsolagem realizada antes e depois de diferentes sistemas de preparo periodico do solo". Spanish. In: *Ciencia Rural* 39.9, pp. 2501–2506. ISSN: 01038478. URL: https://link.gale.com/apps/doc/A442117716/IFME?u=anon~7f23e826&sid=googleScholar&xid=98b4c0b5.

Schäffer, B., W. Attinger, and R. Schulin (2007). "Compaction of restored soil by heavy agricultural machinery-Soil physical and mechanical aspects". In: *Soil and Tillage Research* 93.1, pp. 28–43. ISSN: 01671987. DOI: 10.1016/j.still.2006.03.007.

Schindelin, J., I. Arganda-Carreras, E. Frise, V. Kaynig, M. Longair, T. Pietzsch, S. Preibisch, C. Rueden, S. Saalfeld, B. Schmid, J.-Y. Tinevez, D. J. White, V. Hartenstein, K. Eliceiri, P. Tomancak, and A. Cardona (2012). "Fiji: an open-source platform for biological-image analysis". In: *Nature Methods* 9.7, pp. 676–682. ISSN: 1548-7091. DOI: 10.1038/nmeth.2019. URL: http://www.nature.com/articles/nmeth.2019.

Schjønning, P., J. J.H. van den Akker, T. Keller, M. H. Greve, M. Lamandé, A. Simojoki, M. Stettler, J. Arvidsson, and H. Breuning-Madsen (2015). "Driver-Pressure-State-Impact-Response (DPSIR) analysis and risk assessment for soil compaction-A European perspective". In: *Advances in Agronomy* 133, pp. 183–237. ISSN: 00652113. DOI: 10.1016/bs.agron.2015.06.001.

Schjønning, P., I. K. Thomsen, P. Moldrup, and B. T. Christensen (2003). "Linking Soil Microbial Activity to Water- and Air-Phase Contents and Diffusivities". In: *Soil Science Society of America Journal* 67.1, pp. 156–165. ISSN: 03615995. DOI: 10.2136/sssaj2003.1560. URL: http://doi.wiley.com/10.2136/sssaj2003.1560.

Schneider, F., A. Don, I. Hennings, O. Schmittmann, and S.J. Seidel (2017). "The effect of deep tillage on crop yield – What do we really know?" In: *Soil and Tillage Research* 174.July, pp. 193–204. ISSN: 01671987. DOI: 10.1016/j.still.2017.07.005. URL: http://dx.doi.org/10.1016/j.still.2017.07.005.

Sinnett, D., J. Poole, and T. R. Hutchings (2006). "The efficacy of three techniques to alleviate soil compaction at a restored sand and gravel quarry". In: *Soil Use and Management* 22.4, pp. 362–371. ISSN: 02660032. DOI: 10.1111/j.1475-2743.2006.00053.x.

Soane, G.C., R.J. Godwin, MJ. Marks, and G. Spoor (1987). "Crop and soil response to subsoil loosening, deep incorporation of phosphorus and potassium fertilizer and subsequent soil management on a range of soil types.: Part 2: Soil structural conditions". In: *Soil Use and Management* 3.3, pp. 123–130. ISSN: 0266-0032. DOI: 10.1111/j.1475-2743.1987.tb00721.x. URL: https://onlinelibrary.wiley.com/doi/10.1111/j.1475-2743.1987.tb00721.x.

Soto-Gómez, D., L. Vázquez Juíz, P. Pérez-Rodríguez, J. E. López-Periago, M. Paradelo, and J. Koestel (2020). "Percolation theory applied to soil tomography". In: *Geoderma* 357.10, pp. 1–9. ISSN: 00167061. DOI: 10.1016/j.geoderma.2019.113959. URL: https://doi.org/10.1016/j.geoderma.2019.113959.

Spoor, G. (2006). "Alleviation of soil compaction: Requirements, equipment and techniques". In: *Soil Use and Management* 22.2, pp. 113–122. ISSN: 02660032. DOI: 10.1111/j.1475-2743.2006.00015.x.

Spoor, G., F. G.J. Tijink, and P. Weisskopf (2003). "Subsoil compaction: Risk, avoidance, identification and alleviation". In: *Soil and Tillage Research* 73.1-2, pp. 175–182. ISSN: 01671987. DOI: 10.1016/S0167-1987(03)00109-0.

Stepniewski, W. (1980). "Oxygen-diffusion and strength as related to soil compaction. I. ODR." In: *Polish Journal of Soil Science* 13.1, pp. 3–13. URL: https://www.cabdirect.org/cabdirect/abstract/19821968418.

Stonestrom, D. A. and J. Rubin (1989). "Air permeability and trapped-air content in two soils". In: *Water Resources Research* 25.9, pp. 1959–1969. ISSN: 00431397. DOI: 10.1029/WR025i009p01959. URL: http://doi.wiley.com/10.1029/WR025i009p01959.

Swisstopo (2022). "Maps of Switzerland - Swiss Confederation". geo.admin.ch, [last accessed: 24.08.2022]. URL: https://map.geo.admin.ch/?lang=de&topic=ech&bgLayer=ch.swisstopo.pixelkarte-farbe&layers=ch.swisstopo.zeitreihen,ch.bfs.gebaeude_wohnungs_register,ch.bav.haltestellen-oev,ch.swisstopo.swisstlm3d-wanderwege,ch.astra.wanderland-sperrungen_umleitungen&layers.

Switzerland, Bundesrat (1998). *Verordnung über Belastungen des Bodens (VBBo)*.

Switzerland, Bundesversammlung der Schweizerischen Eidgenossenschaft (1983). *Bundesgesetz über den Umweltschutz*.

Tarawally, M. A., H. Medina, M. E. Frómeta, and C. A. Itza (2004). "Field compaction at different soil-water status: effects on pore size distribution and soil water characteristics of a Rhodic Ferralsol in Western Cuba". In: *Soil and Tillage Research* 76.2, pp. 95–103. ISSN: 01671987. DOI: 10.1016/j.still.2003.09.003. URL: https://linkinghub.elsevier.com/retrieve/pii/S0167198703002241.

Volkmar, K. M. (1996). "Effects of biopores on the growth and N-uptake of wheat at three levels of soil moisture". In: *Canadian Journal of Soil Science* 76.4, pp. 453–458. ISSN: 0008-4271. DOI: 10.4141/cjss96-056. URL: http://www.nrcresearchpress.com/doi/10.4141/cjss96-056.

Wahlström, E. M., H. L. Kristensen, I. K. Thomsen, R. Labouriau, M. Pulido-Moncada, J. A. Nielsen, and L. J. Munkholm (2021). "Subsoil compaction effect on spatio-temporal root growth, reuse of biopores and crop yield of spring barley". In: *European Journal of Agronomy* 123.5. ISSN: 11610301. DOI: 10.1016/j.eja.2020.126225.

Weil, R. R. and N.C. Brady (2017). "Soil organic matter". In: *The nature and properties of soil*. 15th ed. Essex: Person Education. Chap. 11, pp. 1–1104. ISBN: 1292162236.

Wiermann, C., D. Werner, R. Horn, J. Rostek, and B. Werner (2000). "Stress/strain processes in a structured unsaturated silty loam Luvisol under different tillage treatments in Germany". In: *Soil and Tillage Research* 53.2, pp. 117–128. ISSN: 01671987. DOI: 10.1016/S0167-1987(99)00090-2. URL: https://linkinghub.elsevier.com/retrieve/pii/S0167198799000902.

Zhai, X. and R. Horn (2019). "Dynamics of pore functions and gas transport parameters in artificially ameliorated soils due to static and cyclic loading". In: *Geoderma* 337, pp. 300–310. ISSN: 00167061. DOI: 10.1016/j.geoderma.2018.09.039. URL: https://linkinghub.elsevier.com/retrieve/pii/S0016706118307225.

Zhang, Y., A. E. Hartemink, J. Huang, and B. B. T. Minasny (2021). "Digital Soil Morphometrics". In: *Reference Module in Earth Systems and Environmental Sciences*. Elsevier, pp. 126–138. ISBN: 978-0-12-409548-9. DOI: https://doi.org/10.1016/B978-0-12-822974-3.00008-2. URL: https://www.sciencedirect.com/science/article/pii/B9780128229743000082.

Declaration of Authorship

Personal declaration: I hereby declare that the submitted Thesis is the result of my own, independent work. All external sources are explicitly acknowledged in the Thesis. I confirm that:

- This work was done wholly or mainly while in candidature for a research degree at this University.
- Where any part of this thesis has previously been submitted for a degree or any other qualification at this University or any other institution, this has been clearly stated.
- Where I have consulted the published work of others, this is always clearly attributed.
- Where I have quoted from the work of others, the source is always given. With the exception of such quotations, this thesis is entirely my own work.
- I have acknowledged all main sources of help.
- Where the thesis is based on work done by myself jointly with others, I have made clear exactly what was done by others and what I have contributed myself.

Signed: A. Widmer

Date: 25.08.2022